Chen, Yuzhu; Xu, Jinzhao; Zhao, Dandan; Wang, Jun; Lund, Peter D.

Exergo-economic assessment and sensitivity analysis of a solar-driven combined cooling, heating and power system with organic Rankine cycle and absorption heat pump

Published in:
Energy

DOI:
10.1016/j.energy.2021.120717

Published: 01/09/2021

Document Version
Peer-reviewed accepted author manuscript, also known as Final accepted manuscript or Post-print

Exergo-economic assessment and sensitivity analysis of a solar-driven combined cooling, heating and power system with organic Rankine cycle and absorption heat pump

Yuzhu Chen [a], Jinzhao Xu [a], Dandan Zhao [a], Jun Wang [a*], Peter D. Lund [a, b*]

[a] School of Energy and Environment, Southeast University, No 2 Si Pai Lou, Nanjing, 210096, China

[b] School of Science, Aalto University, P.O. Box 15100, FI-00076, Aalto (Espoo), Finland

∗ Corresponding authors: Jun Wang; e-mail: 101010980@seu.edu.cn; Peter D. Lund; e-mail: peter.lund@aalto.fi

Abstract

District energy systems based on renewable resources help to reduce greenhouse-gas emissions and fossil-fuel use. Here, a tri-generation energy system combining cooling, heating, and power is realized by employing organic Rankine cycle (ORC) and absorption heat pump (AHP) technologies, which enable cascading the utilization of solar heat. The AHP can operate steadily providing cooling, heating and hot water from solar thermal and geothermal sources. A modelling approach presented to evaluate the energy, exergy, economic, and exergo-economic performance of the above system. The results show that the AHP could reach a coefficient of performance (COP) between 1.38-2.37 depending on the mode of operation. The yearly energy and exergy efficiency of the tri-generation system is 56.5% and 9.6%, respectively. Compared to a separate system, the simple economic payback time of the tri-generation system is 3.5 years. The specific exergo-economic cost of electricity produced is 0.12 $/kWh, whereas the cost of hot water is much higher, or 0.31 $/kWh. The sensitivity analysis performed shows that the inlet and outlet temperatures of the AHP together with the yearly solar irradiance have the highest impact on the performance. This study provides a new direction on cost-effective utilization of renewable sources in district energy systems.

Keywords: trigeneration, combined cooling, heating and power, parabolic trough collectors, absorption heat pump, exergo-economic analysis, sensitivity analysis

Nomenclature

AHP	Absorption heat pump
CCHP	Combined cooling, heating and power
CCP	Combined cooling and power
COP	Coefficient of performance
HG	High-pressure generator
HTX	High-temperature heat exchanger
LG	Low-pressure generator
LTX	Low-temperature heat exchanger
ORC	Organic Rankine cycle
PTC	Parabolic trough collector
ST	Steam turbine

Symbols

A	Area, m^2
C	Cost, $
CRF	Capital recovery factor
Cx	Capital investment, $
E	Electricity, kWh
EL	Energy level
I_b	Solar irradiance, W/m^2
Ex	Exergy, kWh
h	Enthalpy, kJ/kg
H	Operating time, hours
PP	Payback period, years
s	Entropy, kJ/K
SL	Service life, years
Sv	Cost savings, $
$LMTD$	Logarithmic mean temperature difference
U	Heat transfer coefficient, $kW/(m^2 K)$
Z	Levelized capital cost, $
σ	Interest rate, %
η	Efficiency, %
ε	Ratio
λ	Maintenance cost ratio
θ	Specific cost of geothermal water, $/t
ω_{grid}	Cost of grid electricity, $/kWh

Superscript/ Subscript

cap	Capital
con	Condenser
cool	Cooling condition
CW	Chilled water
CI	Levelized hourly investment cost
DHW	Domestic hot water
en	Energy
eva	Evaporator
f	Fuel
geo	Geothermal
heat	Heating
HW	Space heating water
i	i^{th} unit of ORC
in/out	Inlet/outlet
invest	Investment
k	k^{th} unit
$loss$	Loss
main	Maintenance

m	Mass flow, kg/s	nom	Nominal
Q	Thermal energy, kWh	p	Product
$SPEC$	Specific cost of chilled water, $/kWh	reg	Regenerator
T	Temperature, °C	transition	Transition condition

1 Introduction

Buildings accounts for 30% of total energy use [1]. District energy systems that employ local renewable energy sources such as solar energy [2] could bring major benefits in energy, environmental, and economic performance.

Solar energy can be utilized as thermal [3], electric [4] or chemical [5] energy forms. For solar thermal utilization different types of solar collectors [6] are available for different temperature level requirements. These include evacuated tube, flat plate, parabolic trough (PTC) and paraboloid dish collectors. For solar electricity production, photovoltaic systems are typically employed [7] mainly based on silicon solar cells, though other cell types such as thin film cells also exist. Typical end-use applications of solar energy include refrigeration [8], heating [9], power generation [10], and thermochemical [11] uses, but these can also be integrated into combined cooling and power (CCP) [12], combined heat and power (CHP) [13], and combined cooling, heating and power (CCHP), or, tri-generation systems [14], to generate multiple services to building loads to realize near zero or even zero fossil fuel energy systems.

Contrary to combined heat and power systems, which contain power generation modules and heat exchanger modules, more sophisticated technologies are needed when adding cooling to the system [15]. In CCP and CCHP systems, absorption, adsorption, ejector, compression and other refrigeration technologies are required. Compression cooling operates on electric power and reaches the highest energy level [16], while the other three methods employ thermal energy. In solar-driven CCHP systems, ejector refrigeration is more widely used than solar adsorption and absorption processes. In a conventional solar thermal CCHP system with ejector cooling, the main system components include the solar collectors [17], ejector, and the Rankine cycle engine. Most of the analyses on CCP and CCHP systems have focused on thermodynamic performance [18], multi-objective optimization [12], and economic performance [19]. A levelized energy cost of $\$15.3GJ^{-1}$ has been reported for an optimized CCHP system with ejector cooling and Rankine units with supercritical CO_2 and N_2O as working

media [19]. However, the coefficient of performance (COP) of ejector cooling is low, similar to adsorption cooling. A COP of 0.64 has been reported for a solar adsorption cooling CCHP system [20] with a maximum adsorption energy efficiency of 4.3% only [21].

To ensure a higher energy performance, an absorption chiller with higher COP is preferred in solar driven district energy systems [22]. With a single-effect absorption chiller, the payback-time of PTC-driven CCHP systems could be less tan 10 years [23]. High energy efficiencies up to 87-93% have been reported for solar-powered trigeneration systems [24] with double-effect chiller, with an exergy efficiency in the range of 6.6% -12.7%. A system with two single-effect chillers could reach an energy efficiency of 98% and exergy efficiency of 17% in summer conditions [25]. The solar CCHP system can also be parallel connected with a double-effect absorption chiller with a higher COP. For such a CCHP system a minimum exergo-economic cost of 0.83 $/kWh has been reported, when 86% and 14% of the solar heat was fed to the ORC and absorption units y [26]. However, it was found that the COP of the absorption unit decreases for solar irradiance > 500 W/m^2. To overcome this problem, the absorption unit could be connected in series with the ORC-unit. This type is also the main subject of this paper.

To explore the performance and feasibility of the proposed system in more detail, a set of indicators and criteria are useful such as energy, exergy, economic and environmental performance [27]. Frequently used economic criteria include the annual cost saving ratio [28], payback-time [29], and specific costs of products [30], etc. The payback-time gives an estimate of the required time for the return on investment, whereas the specific cost, especially the specific exergo-economic [26] and thermo-ecological cost [31], can search the specific cost of multiple products based on particular cost allocation method. Here the payback-time and the specific exergo-economic cost were selected for the energy and exergy analysis.

To increase the share of renewable sources and to reduce the fossil fuel use and emissions, solar and geothermal energy is employed in this study through a novel solar-driven CCHP system. The original features of the proposed CCHP system are as follows: (1) The hybrid system is constructed by cascading the utilization of solar energy to generate four main products: solar heat at higher temperature is used to drive the ORC, while the waste heat is absorbed by the AHP; (2) the ORC-unit with a regenerator can produce both power and hot water; a double-effect absorption heat pump is utilized to generate cooling, hot water, and heating in different conditions over the whole year; (3)

geothermal energy is utilized as cooling water during the cooling demand, but also for the heating demand. The payback-time of the system is analyzed and compared to other relevant studies. The exergo-economic cost of the energy services is evaluated for different working modes and Chinese cities with different climatic conditions.

2 Solar driven combined cooling, heating and power system

The layout, flowcharts and thermal models of the hybrid CCHP system are illustrated in Sections 2.1 and 2.2.

2.1 Layout of hybrid system

The energy flowchart of the hybrid CCHP system is explained in Fig. 1. The CCHP system consists of three main units: concentrating solar thermal device (PTC), organic Rankine Cycle and absorption heat pump (AHP) unitc.

In Fig. 1(a), the PTCs convert solar irradiance into thermal energy and heat up the working fluid (state 1). The outlet steam (state 2) with a higher temperature is fed to the ORC and AHP to generate cooling (state 8), heating (state 4), electricity (state 6) and domestic hot water (states 7, 5) to fulfill the building energy demands.

Observing the energy flowcharts of the ORC [32] in Fig. 1(b), the organic medium (state b1) isopentane is evaporated to a higher-pressure and higher-temperature state (state b2) by absorbing solar thermal energy. After performing work in the steam turbine (ST), the medium (state b5) releases its heat in the regenerator. Then, the outlet medium (state b6) is continuing to be condensed in a condenser with a condensation temperature of 60°C (state b7). After the compressing and preheating processes in the pump and regenerator, the organic medium is returned to its original state (state b1) for the next cycle. In the ORC-unit, the electricity is generated by the generator and the tap water (state 11, 25°C) is used as the cooling water to absorb the heat released in the condenser and to generate domestic hot water (state 5, 40°C).

The energy flowchart of the absorption heat pump is displayed in Fig. 1(c). The flows of the LiBr solution and refrigeration vapor are explained in [33]. Due to the different building demands for the whole year [34], the AHP in this study is utilized to produce chilled water (7°C/12°C), domestic hot water (40°C/25°C), and space heating water (40°C/35°C) in cooling, transition, and heating conditions,

respectively.

In the cooling conditions, the evaporator of the AHP can absorb heat from returned chilled water (12°C). The geothermal water with an inlet temperature of 25°C is used to absorb the excess heat in the absorber and condenser of the AHP, while the outlet temperature is set at 30°C. In the transition conditions, domestic hot water is produced by heating the tap water in the absorber and condenser. The geothermal water works now as a lower-temperature heat resource to release heat in the evaporator, with inlet at 25°C and outlet at 20°C. The flows of the AHP in the heating mode are similar to the flows in the transition mode; the return heating water (35°C) is heated in the absorber and condenser by absorbing solar thermal and geothermal heat.

In summary, the proposed CCHP system can generate chilled water in the cooling conditions, space heating water in the heating conditions, and domestic hot water and electricity in all conditions.

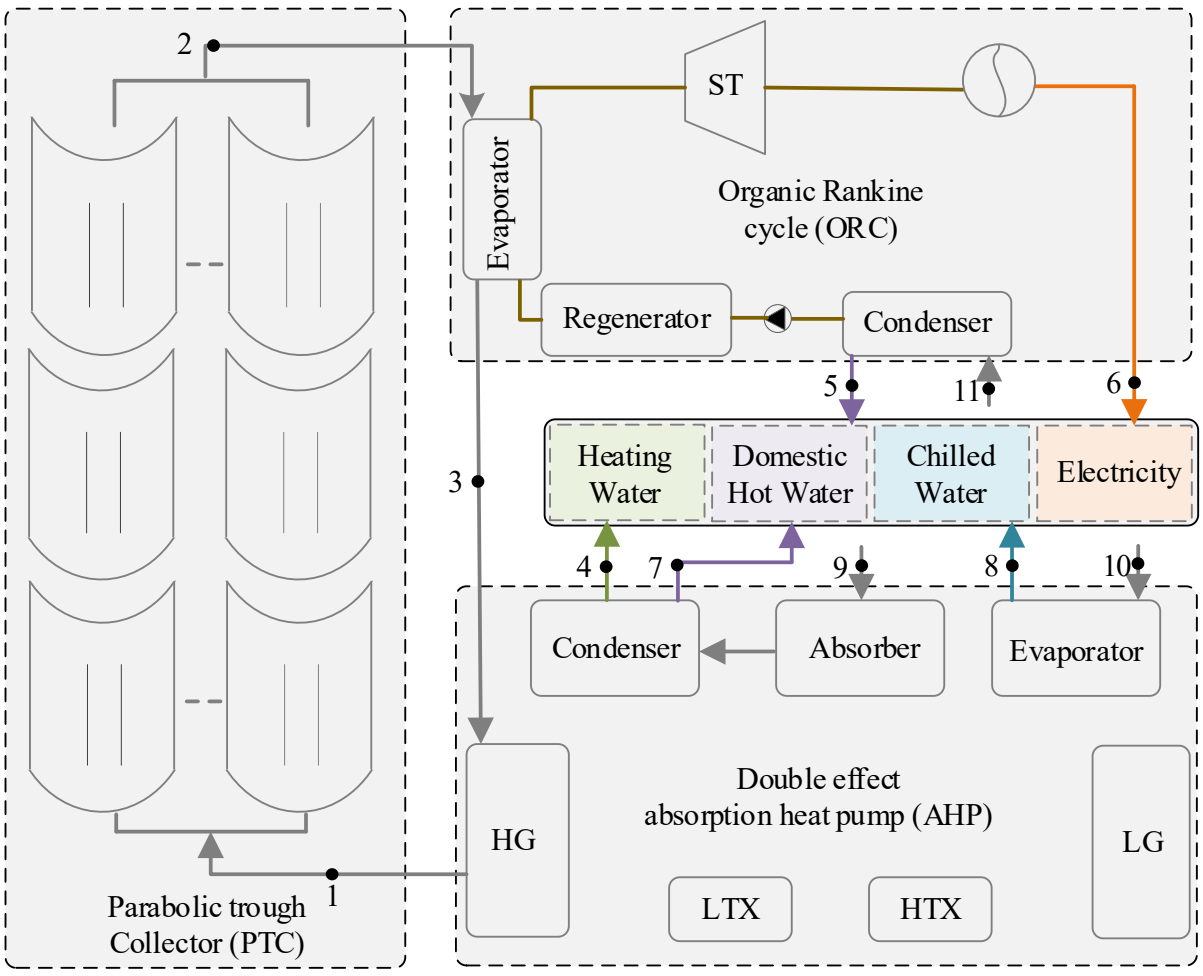

(a) Combined cooling heating and power system

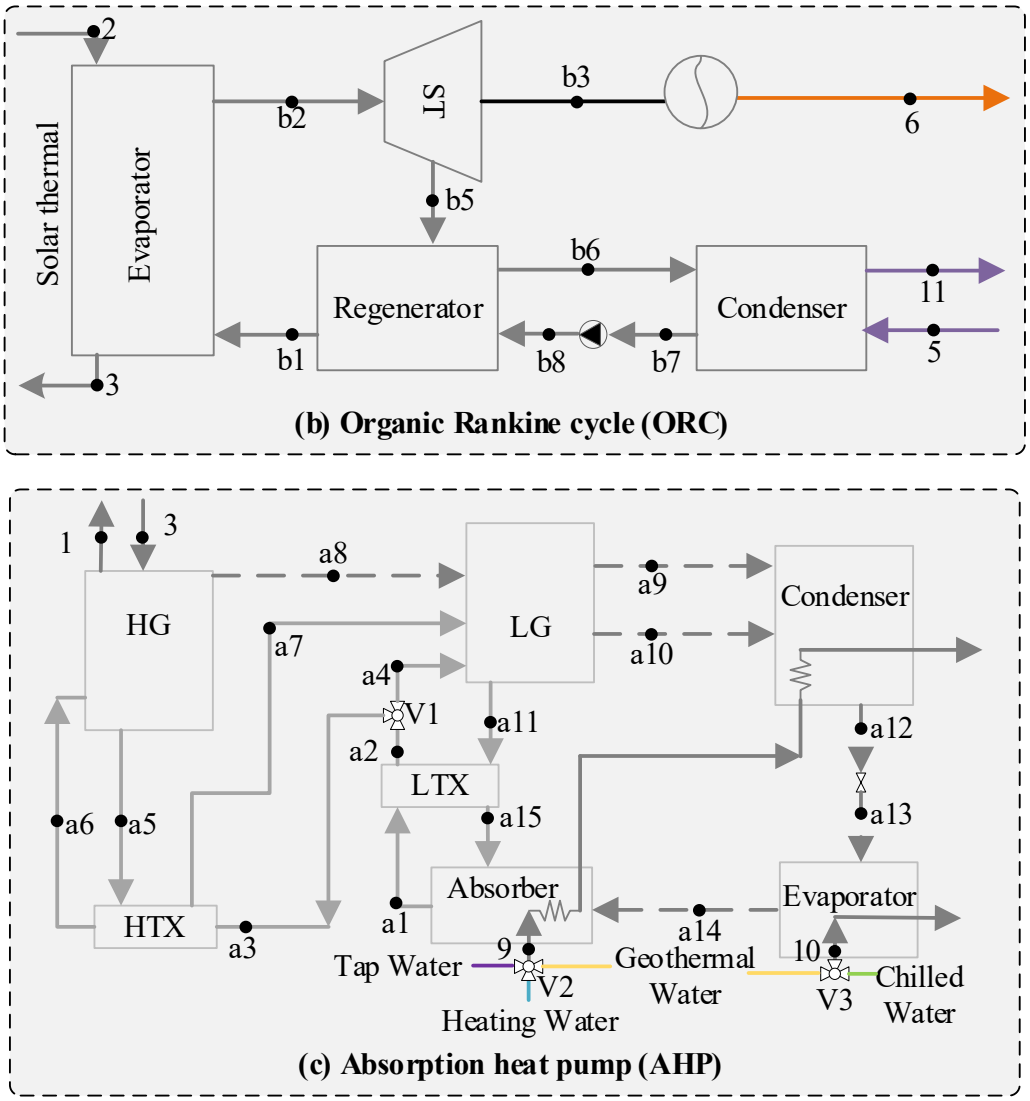

Fig. 1. Energy flows of combined cooling, heating and power system driven by parabolic trough collectors: (a) CCHP system, (b) ORC unit, (c) AHP unit.

2.2 Modelling of the units

When constructing the mathematical models for the components, the following assumptions were applied [35]:

(1) Steady state conditions are assumed in the simulation and analysis;

(2) Heat losses of the components in the ORC and AHP are ignored;

(3) Ancillary electricity consumption of the AHP is ignored;

(4) Countercurrent heat exchange is used in all heat transfer components;

(5) Pressure and temperature in standard condition is 101 kPa and 25°C (T_0);

(6) Pipeline connections are ignored;

(7) Outlet states of the evaporator, condenser in the ORC and AHP, and the outlet solution of the generators and absorber in the AHP are set to statured condition.

The main equations of the PTC, ORC, and AHP are summarized in Table 1.

Table 1. Main thermodynamic models of the units.

Unit	Energy/exergy balances	Other equations	Ref
PTC	$Q_{in,PTC} = Q_{2/1} + Q_{loss,PTC}$	$\eta_{en,PTC} = [74.08 - 4.32(\frac{T_1 - T_0}{I_b}) - 0.05 I_b (\frac{T_1 - T_0}{I_b})^2]\%$	[36]
	$Ex_{in,PTC} = Ex_{2/1} + Ex_{loss,PTC}$	$\eta_{ex,PTC} = 100\% Ex_{2/1} / Ex_{in,PTC}$	
ORC	$Q_{2/3} = E_6 + Q_{5/11} + Q_{loss,ORC}$	$Q_i^{ORC} = U_i^{ORC} A_i^{ORC} LMTD_i^{ORC}$	[32]
	$Ex_{2/3} = E_6 + Ex_{5/11} + Ex_{loss,ORC}$	$\eta_{en,ORC} = 100\%(E_6 + Q_{5/11}) / Q_{2/3}$	
		$\eta_{ex,ORC} = 100\%(E_6 + Ex_{5/11}) / Ex_{2/3}$	
AHP	$\begin{Bmatrix} Q_{1/3} + Q_{8/10} = Q_{geo} + Q_{loss,AHP}(\text{Cooling}) \\ Q_{1/3} + Q_{geo} = Q_{7/9} + Q_{loss,AHP}(\text{Transition}) \\ Q_{1/3} + Q_{geo} = Q_{4/9} + Q_{loss,AHP}(\text{Heating}) \end{Bmatrix}$	$\eta_{en,AHP} = 100\% \begin{Bmatrix} Q_{geo} / (Q_{1/3} + Q_{8/10})(\text{Cooling}) \\ Q_{7/9} / (Q_{geo} + Q_{1/3})(\text{Transition}) \\ Q_{4/9} / (Q_{geo} + Q_{1/3})(\text{Heating}) \end{Bmatrix}$	[37]
	$\begin{Bmatrix} Ex_{1/3} + Ex_{8/10} = Ex_{geo} + Ex_{loss,AHP}(\text{Cooling}) \\ Ex_{1/3} + Ex_{geo} = Ex_{7/9} + Ex_{loss,AHP}(\text{Transition}) \\ Ex_{1/3} + Ex_{geo} = Ex_{4/9} + Ex_{loss,AHP}(\text{Heating}) \end{Bmatrix}$	$\eta_{ex,AHP} = 100\% \begin{Bmatrix} Ex_{geo} / (Ex_{1/3} + Ex_{8/10})(\text{Cooling}) \\ Ex_{7/9} / (Ex_{geo} + Ex_{1/3})(\text{Transition}) \\ Ex_{4/9} / (Ex_{geo} + Ex_{1/3})(\text{Heating}) \end{Bmatrix}$	
		$COP_{AHP} = \begin{Bmatrix} Q_{8/10} / Q_{1/3}(\text{Cooling}) \\ Q_{7/9} / Q_{1/3}(\text{Transition}) \\ Q_{4/9} / Q_{1/3}(\text{Heating}) \end{Bmatrix}$	

where T, I_b, Q, Ex, E, and $LTMD$ are the temperature, solar irradiance, energy, exergy, electricity, and logarithmic mean temperature difference, respectively. η, COP are the efficiency, and coefficient of performance. U and A are the heat transfer coefficient and heat transfer area. The subscript numbers correspond to the states in Fig. 1. i is the i^{th} component; Q_{geo} and Q_{loss} is the geothermal energy and energy loss, respectively.

To evaluate the accuracy of the models, the simulation results are compared to reference studies with the same initial parameters. A commercial PTC-unit Eurotrough II [36] is selected for the solar collector in the validation. The energy efficiency of the PTC ($\eta_{en,PTC}$)is based on an empirical formula [36]. With 1 MW capacity and 60°C condensation temperature, the power generation efficiency is 17.1% in present study, with a relative error of < 0.3% compared to [32]. Compared to [37], the root-mean-square error of pressure, mass flow, temperature, and concentration of the LiBr-unit are 2.3%, 0.5%, 5.1%, and 0.02%, respectively. This demonstrates adequate accuracy of the models.

3 Evaluation methods

A set of evaluation criteria related to energy, exergy and economic are defined in the next to analyze the performance of the proposed CCHP system .

3.1 Energy analysis

Based on the description of the CCHP system in Section 2, the energy outputs from the system in different conditions are as follows:

(1) Chilled water, domestic hot water, and electricity in cooling conditions;

(2) Domestic hot water and electricity in transition conditions;

(3) Space heating water, domestic hot water, and electricity in heating conditions.

Thus, the energy performance is highly affected by the working conditions. The shares of the working conditions are defined as the working hours in the specific conditions of the total working hours:

$$\varepsilon_{cool}=\frac{H_{cool}}{H_{cool}+H_{transition}+H_{heat}} \tag{1}$$

$$\varepsilon_{transition}=\frac{H_{transition}}{H_{cool}+H_{transition}+H_{heat}} \tag{2}$$

$$\varepsilon_{heat}=1-\varepsilon_{cool}-\varepsilon_{transition} \tag{3}$$

where ε_{cool}, $\varepsilon_{transition}$, ε_{heat} are the shares of cooling, transition and heating conditions, respectively.

H_{cool}, $H_{transition}$, H_{heat} are the operating hours of cooling, transition and heating conditions.

The energy inputs (Q_{out}) and outputs (Q_{in}) of three working conditions are expressed by the following equations:

$$Q_{out}=\begin{cases}\varepsilon_{cool}(Q_{8/10}+E_6^{cool}+Q_{5/11}^{cool})+\\ \varepsilon_{transition}(Q_{7/9}+E_6^{transition}+Q_{5/11}^{transtion})+\\ \varepsilon_{heat}(Q_{4/9}+E_6^{heat}+Q_{5/11}^{heat})\end{cases} \tag{4}$$

$$Q_{in}=\begin{cases}\varepsilon_{cool}(Q_{1/3}^{cool}+Q_{geo}^{cool})+\\ \varepsilon_{transition}(Q_{1/3}^{transition}+Q_{geo}^{transition})+\\ \varepsilon_{heat}(Q_{1/3}^{heat}+Q_{geo}^{heat})\end{cases} \tag{5}$$

The energy efficiency ($\eta_{en,sys}$) of the proposed system can then be determined as the ratio of energy outputs to energy inputs [27]:

$$\eta_{en,sys}=100\%\frac{Q_{out}}{Q_{in}} \tag{6}$$

3.2 Exergy analysis

Similar to the energy analysis in Section 3.1, the exergy input, output and exergy efficiency of the hybrid system can be calculated as follows [38]:

$$Ex_{out}=\begin{cases}\varepsilon_{cool}(Ex_{8/10}+E_6^{cool}+Ex_{5/11}^{cool})+\\ \varepsilon_{transition}(Ex_{7/9}+E_6^{transition}+Ex_{5/11}^{transtion})+\\ \varepsilon_{heat}(Ex_{4/9}+E_6^{heat}+Ex_{5/11}^{heat})\end{cases} \tag{7}$$

$$Ex_{in}=\begin{cases}\varepsilon_{cool}(Ex_{1/3}^{cool}+Ex_{geo}^{cool})+\\ \varepsilon_{transition}(Ex_{1/3}^{transition}+Ex_{geo}^{transition})+\\ \varepsilon_{heat}(Ex_{1/3}^{heat}+Ex_{geo}^{heat})\end{cases} \tag{8}$$

$$\eta_{ex,sys}=100\%\frac{Ex_{out}}{Ex_{in}} \tag{9}$$

where Ex_{out}, Ex_{in}, and $\eta_{en,sys}$ are the outlet exergy, inlet exergy and exergy efficiency of the CCHP system, respectively.

3.3 Economic analysis

The economic performance is crucial to assess in order to improve the cost-effectiveness of the system. In this study, the simple payback-time and exergo-economic methods were selected for this purpose.

3.3.1 Payback-time analysis

The payback period (*PP*) gives a quick estimate of the economic viability of the system, though ignoring the time value of cost. It is calculated as follows [39]:

$$PP = \frac{Cx}{Sv} \tag{10}$$

where Cx (Table 2), and Sv are the capital investment and monetary savings/revenues from the hybrid system, respectively.

In the calculation of the savings (Sv), separate systems are used to produce the poly-products: the cooling is generated by the electric chiller (COP= 3) [40], the heating and domestic hot water are produced by an electric heater with an efficiency of 95% [41], and the electricity load is met by the power grid. Thus, the savings of the hybrid system over a year is equal to the cost of grid electricity consumption of the reference system:

$$Sv = (E_{CW}^{ref} + E_{DHW}^{ref} + E_{HW}^{ref} + E_{E}^{ref})\omega_{grid} \tag{11}$$

where E_{cool}^{ref}, E_{DHW}^{ref}, E_{heat}^{ref} and E_{E}^{ref} is the grid electricity consumption for the cooling, domestic hot water, heating and electricity loads, respectively. ω_{grid} represents the cost of grid power, which is here 0.129 \$/kWh [9]. Subscripts CW, HW and DHW represent chilled water, space heating water and domestic hot water, respectively.

3.3.2 Exergo-economic analysis

Based on the exergy analysis, the exergo-economic cost of each state of the energy system can be assessed by the cost allocation method [42]. The exergo-economic cost of the product (C_p) is related to the fuel exergy cost and investment cost:

$$\sum(C_p)_k=\sum(C_f)_k+Z_k \tag{12}$$

where C_f, and Z is the fuel exergy cost rate and hourly levelized investment cost. k is k^{th} unit of the energy system.

The hourly levelized investment cost is mainly affected by the operating hours (H), service life (SL), capital investment cost (Z^{cap}), maintenance cost (Z^{main}), and interest rate (σ):

$$Z_k = Z_k^{CI} + Z_k^{main} \tag{13}$$

$$Z_k^{main} = \lambda Z_k^{CI} \tag{14}$$

$$Z_k^{main} = \frac{Z_k^{cap} CRF}{H} \tag{15}$$

$$CRF = \frac{\sigma(1+\sigma)^{SL}}{(1+\sigma)^{SL}-1} \tag{16}$$

where Z^{CI}, λ, and CRF are the levelized hourly investment cost, maintenance cost ratio and cash recovery factor. The investment costs of the subsystems in this study are summarized in Table 2.

Table 2. Investment cost of subsystems.

Unit	Component	Investment cost, $	Ref.
PTC		$13925(A_{PTC})^{0.17}$	[43]
AHP		$482(Q_{nom})^{0.93}-159.7Q_{nom}$	[44]
ORC	Evaporator	$276(A_{eva})^{0.88}$	[45]
	Steam turbine (ST)	$4750(E_{nom})^{0.75}+60(E_{nom})^{0.95}$	[45]
	Regenerator	$130(A_{reg}/0.093)^{0.78}$	[45]
	Condenser	$150(A_{con})^{0.8}$	[45]
	Pump	$3500(E_{pump})^{0.41}$	[45]

The energy level (EL) of the product, which is related to entropy (ΔS) and enthalpy (ΔH)

differences, is taken into consideration to reasonably evaluate the exergo-economic performance of multi-products [46]:

$$EL = 1 - T_0 \frac{\Delta S}{\Delta H} \tag{17}$$

For the PTC-unit, the cost of solar irradiance is free (C_{I_b}), and the exergo-economic equation can be expressed as:

$$C_{I_b} + Z_{PTC} = C_{1/2} \tag{18}$$

For the ORC, the fuel cost is $C_{1/2}$, and the product cost includes the solar steam to AHP unit ($C_{2/3}$), the domestic hot water ($C_{5/11}$), and the electricity (C_6) are as follows:

$$C_{1/2} + Z_{ORC} = C_{2/3} + C_{5/11} + C_6 \tag{19}$$

$$\frac{C_{2/3} Ex_{5/11}}{C_{5/11} Ex_{2/3}} = \frac{EL_{2/3}}{EL_{5/11}} \tag{20}$$

$$\frac{C_{2/3} Ex_6}{C_6 Ex_{2/3}} = \frac{EL_{2/3}}{EL_6} \tag{21}$$

For the AHP, the fuel cost is the cost of the solar steam ($C_{2/3}$) and geothermal water (C_{geo}). The product cost of the AHP is affected by the working conditions as follows:

$$C_{2/3} + C_{geo} + Z_{AHP} = \begin{cases} C_{8/10}(\text{Cooling}) \\ C_{7/9}(\text{Transition}) \\ C_{4/9}(\text{Heating}) \end{cases} \tag{22}$$

$$C_{geo} = m_{geo} \theta_{geo} \tag{23}$$

where m_{geo}, θ_{geo} are the mass flow of geothermal water, and the specific cost of geothermal water (0.0195 $/t) [47].

Furthermore, the specific cost of multi-products [42] containing chilled, heating, domestic hot water, and electricity can be determined as follows:

$$SPEC_{CW} = \frac{C_{8/10}}{Ex_{8/10}} \tag{24}$$

$$SPEC_{HW} = \frac{C_{4/9}}{Ex_{4/9}} \tag{25}$$

$$SPEC_{DHW} = \frac{\varepsilon_{cool} C_{5/11}^{cool} + \varepsilon_{transition} C_{5/11}^{transition} + \varepsilon_{heat} C_{5/11}^{heat}}{\varepsilon_{cool} Ex_{5/11}^{cool} + \varepsilon_{transition} Ex_{5/11}^{transition} + \varepsilon_{heat} Ex_{5/11}^{heat}} \tag{26}$$

$$SPEC_{E} = \frac{\varepsilon_{cool} C_{6}^{cool} + \varepsilon_{transition} C_{6}^{transition} + \varepsilon_{heat} C_{6}^{heat}}{\varepsilon_{cool} E_{6}^{cool} + \varepsilon_{transition} E_{6}^{transition} + \varepsilon_{heat} E_{6}^{heat}} \tag{27}$$

where $SPEC$ is the specific cost of the product.

4 Initialization parameters and simulation results

The initial parameters of the proposed CCHP system and simulation results are described in the next.

4.1 Initialization parameters

The weather parameters in Beijing (a cold region in China, year 2015) [9], including the solar irradiance and ambient temperature were obtained from the Energy plus software [48]. The monthly total irradiance and hourly average temperature is shown in Fig. 2. The cooling demand is from 1 May to 31 August, and the heating extends from 1 November to 28 February. During other times, the system works in a transition mode. The solar irradiance for the whole year is almost 1400 kWh/m^2 and the average temperature is 13°C.

Based on the method in [49], the environmental parameters are converted to the three specific conditions to evaluate the performance of the CCHP system in these conditions. The details are as follows:

(1) The solar irradiance level in the cooling, transition and heating conditions are set at 800 W/m^2, 700 W/m^2, and 600 W/m^2, respectively;

(2) Based on (1), the operating hours (H) for the three conditions are 766 hours, 701 hours and 495 hours, the total operating hours for the whole year are 1962 hours. The shares of cooling (ε_{cool}), transition ($\varepsilon_{transition}$), heating (ε_{heat}) conditions are 0.39, 0.36, and 0.25, respectively.

(3) The average temperatures for the three conditions are 24°C, 14°C, and 0°C, respectively.

(4) The service life (SL) is assumed to be 25 years [50], the interest rate is 5% [50], and the

maintenance ratio is 6% [51].

(5) The installed PTC area is 1000 m^2 with a mass flow rate of 3 kg/s.

(6) The geothermal source with an outlet temperature 25°C is used as cooling water and low-temperature source for the AHP with a temperature difference of 5°C.

(7)

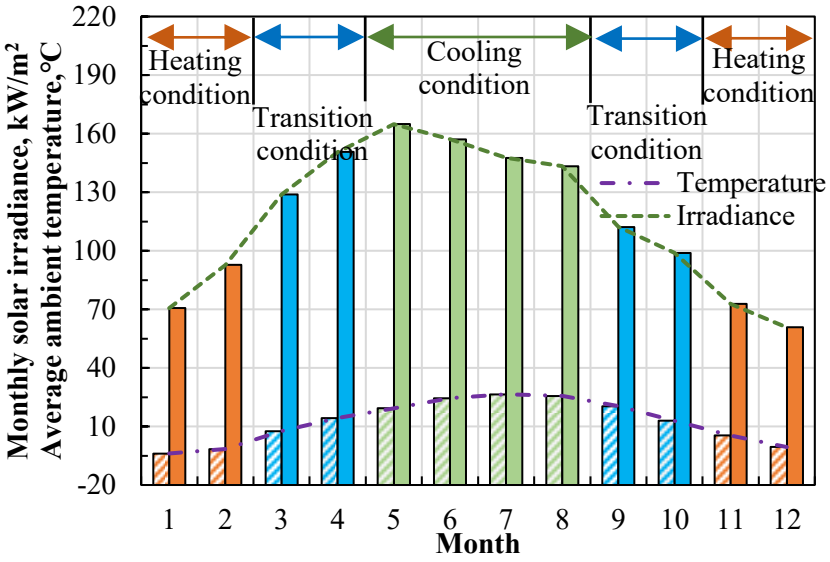

Fig. 2 Average monthly solar irradiance and ambient temperature (weather data is for year 2015 [48]).

4.2 Simulation results

Based on the analysis described above, the energy, exergy and exergo-economic performance for a whole year and different working conditions are presented in the next.

4.2.1 Energy and exergy performance over a whole year

The energy, exergy performance including outputs and efficiencies in both three conditions are displayed in Table 3. While the output of chilled water is 329.0 kWh, the solar irradiance input is 800 kWh. The capacity of space heating water is nearly 1.6 times that of chilled water, but is accompanied by a lower solar input 700 kWh. However, the cooling exergy, 27.0 kWh is 30.43% higher than the heating exergy output, which can be attributed to the higher temperature differences of standard condition, 25°C. In transition condition, the total domestic hot water is 706.3 kWh, with 80.14% output from AHP, and 140.3 kWh from ORC unit. Compared to the exergy out of chilled and heating water

from AHP unit, the exergy of domestic hot water is the lowest, 13.8 kWh, although the energy is the highest. This is mainly due to the lowest energy level caused by the lower inlet/outlet temperature (25°C/40°C). Observing the contributions of ORC, the descending order of total output, including domestic hot water and electricity, is cooling, transition and heating conditions, which results from a lower input solar thermal energy of ORC influenced by the decreasing solar irradiance. During the simulation, the cooling condition obtains lowest energy efficiency, 42.84%, but the highest exergy efficiency, 10.77%. On the other hand, the differences of energy, exergy efficiencies both in transition and heating conditions are lower, although the heating condition has the highest energy efficiency, 67.95%.

Compared to the natural gas fired CCHP system integrated with evacuated tube collector [44], the hybrid CCHP system in this study has lower energy and exergy efficiencies. The energy efficiencies in cooling and heating modes in [44] are 78.7% and 72.9%, and the exergy efficiencies are almost two fold than this study. It can be explained by the lower energy density of solar irradiance.

Table 3. Energy and exergy results in different conditions.

Conditions		Cooling/heating, kWh	Domestic hot water, kWh	Electricity, kWh	Efficiency, %
Cooling condition	Energy	329.0	179.5	49.2	42.8
	Exergy	27.0	4.4	49.2	10.8
Transition condition	Energy	0	706.3	37.9	67.1
	Exergy	0	17.2	37.9	8.4
Heating condition	Energy	514.8	100.6	26.7	67.0
	Exergy	20.7	2.5	26.7	8.9

4.2.2 Economic performance of the CCHP system

The investment cost of a hybrid CCHP system is higher than of the references system, also the installation and maintenance cost could increase. However, during the operational stage, the proposed CCHP system does not use grid electricity leading to major savings. The simple payback-time calculated by Eq. (10) is 3.0 years, which is 9 years lower in [23], which justifies economically the proposed CCHP system. Compared to [44], the payback-time is here also lower as the system in [44] has higher investment cost caused by the internal combustion engine and higher operational due to used of natural gas.

The specific exergo-economic cost of multi-products from ORC and AHP are summarized in

Table 4 using the modified cost allocation method [52]. The specific costs of chilled and space heating are 0.217 $/kWh, and 0.307 $/kWh, respectively. Compared to the other two heat products, the cost of domestic hot water from the AHP is the highest, or, 0.432 $/kWh, due to the higher investment cost of the AHP and the lower exergy output of domestic hot water. Compared to the conventional calculation method in [52], the modified cost is lower or the three main water products. As to the products from the ORC-unit, the specific cost in the heating condition is the highest, 0.074 $/kWh. This can be explained by the higher investment cost of the ORC-unit (Table 2). With the energy level method, the specific cost of domestic hot water is 2.8% of that of the electricity, because the energy level of electricity is equal to 1, while the energy level of domestic hot water is lower due to the lower temperature (Eq. 17). The ranking of the specific cost of the products from the CCHP system in descending order is: The domestic hot water from the AHP, space heating water, chilled water, electricity, and domestic hot water from the ORC.

Compared to CCHP systems driven by natural gas and solar energy [44, 49], the cost of electricity from the ORC in this study is lower than the cost of electricity from an internal combustion engine and photovoltaic/thermal collectors. The specific costs of water products including chilled water, heating water and domestic hot water are also lower. The primary energy in this study is solar irradiance, and it does not include any fuel cost, while in the reference studies, the products are related to the natural gas.

Table 4. Specific exergo-economic cost of multi-products.

Conditions	Output from AHP, $/kWh		Domestic hot water from ORC, $/kWh		Electricity from ORC, $/kWh	
	A	B	A	B	A	B
Cooling condition	0.217	0.291	0.003	0.060	0.106	0.060
Transition condition	0.432	0.581	0.003	0.066	0.126	0.066
Heating condition	0.307	0.404	0.004	0.074	0.156	0.074

A is the method considering energy level, B is the conventional method in [52].

In Table 5, the specific exergo-economic cost in different cities are compared. Four cities in different climatic regions in China were selected: Beijing (cold region), Harbin (extreme cold), Shanghai (hot summer and cold winter), and Guangzhou (hot summer and warm winter). The

environmental parameters containing the solar irradiance and ambient temperature were obtained from [48] for year 2015. During the simulation, the yearly operating period for the different cities are changed to adapt with the different solar irradiance levels. The yearly operating times for Beijing is the highest (1962 hours), followed by Shanghai and Harbin, while the operating times of Guangzhou is the lowest (1621 hours), although the ambient temperature is higher there than in the other cities. It can be found in Table 5 that with higher yearly operating hours the specific cost decreases due to the decreasing levelized hourly cost of the components. The ambient temperature has a lower impact on the exergo-economic performance. Compared to the multiple products from the different units, the specific cost of the domestic hot water from the ORC is the lowest as the products from the AHP are the most expensive ones.

Table 5. Comparison of specific cost for different cities considering the energy level.

City	Mode	Operating time, hours	Ambient temperature,°C	AHP product, $/kWh	DHW from ORC, $/kWh	Electricity, $/kWh
Beijing (116°E, 40°N)	Cooling mode	766	24	0.217	0.003	0.106
	Transition mode	701	14	0.432	0.003	0.126
	Heating mode	495	0	0.307	0.004	0.156
Harbin (127°E,46°N)	Cooling mode	763	20	0.235	0.003	0.118
	Transition mode	653	3	0.472	0.003	0.141
	Heating mode	345	-14	0.338	0.004	0.176
Shanghai (121°E,31°N)	Cooling mode	661	25	0.231	0.003	0.116
	Transition mode	631	17	0.464	0.003	0.138
	Heating mode	499	8	0.331	0.004	0.170
Guangzhou (113°E,22°N)	Cooling mode	553	28	0.249	0.003	0.128
	Transition mode	532	23	0.502	0.004	0.152
	Heating mode	537	16	0.359	0.005	0.188

4.2.3 Energy performance analysis in different conditions

The energy flow diagrams for the three operating conditions are shown in Fig. 3. In three conditions, the PTCs produce 582.6 kWh, 506.8 kWh, and 430.5 kWh per m^2 a year solar thermal energy, with 27.2%, 27.6%, and 28.2% of the solar radiation lost. Because of the constant temperature of solar steam from the ORC (170°C), the output solar thermal energy of ORC unit is equal to 238.5 kWh for allthree modes. The energy of domestic hot water from the ORC in THE three modes is almost

4.7 times the electricity output. The losses of the ORC for the three modes are19.8%, 17.8%, and 15.3% of the input to the ORC. In cooling mode, the AHP can produce 329.0 kWh cooling water, and it needs 501.8 kWh geothermal energy to absorb the excess heat, while only 65.7 kWh of energy is lost. In transition and heating modes, combined with 238.5 kWh of solar thermal energy, 409.4 kWh and 345.0 kWh geothermal energy is needed to heat the domestic hot water (566.0 kWh), and space heating water (514.8 kWh), respectively, whereas 12.6%, and 11.8% of energy is lost. The COP of the AHP in the three modes is 1.38, 2.37, and 2.16, respectively. Compared to the COP in the heating mode, the COP in the transition mode is higher, because of the lower inlet temperature of the absorber (25°C), while the temperature of the return heating water is 35°C. Compared to [44], the COP in the heating mode is nearly 1.5 times higher.

Compared to [44], the solar collectors in this study produce more thermal energy, although the net electrical efficiency of the ORC (8% in the cooling mode) is lower than the efficiency of an internal combustion engine (36.7%). The COP of the AHP in [44] is lower than here, especially in heating mode: The COP in the heating mode here is almost 1.6 times higher, because the AHP in [44] works only as a heat exchanger.

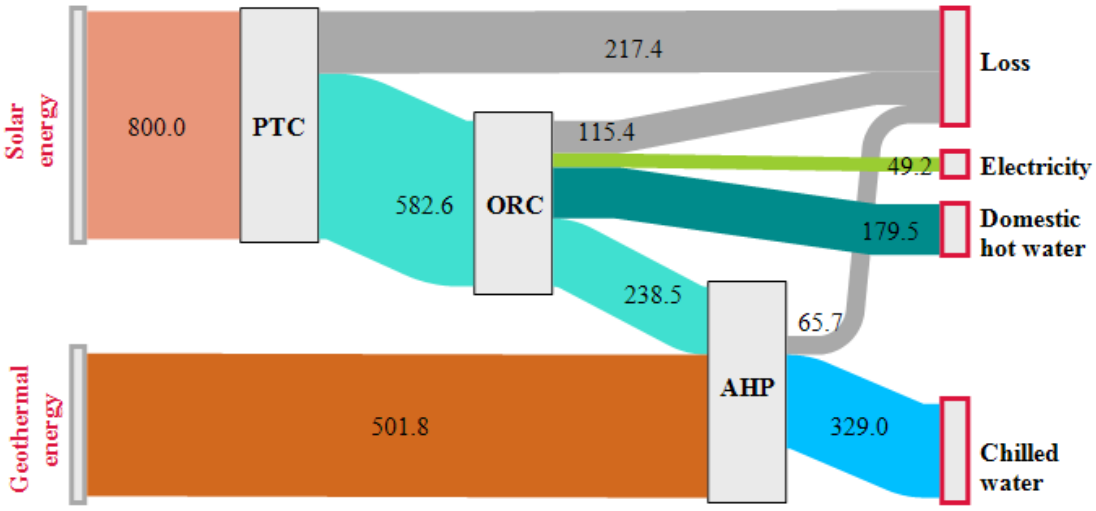

(a) Energy flows in cooling condition, kWh

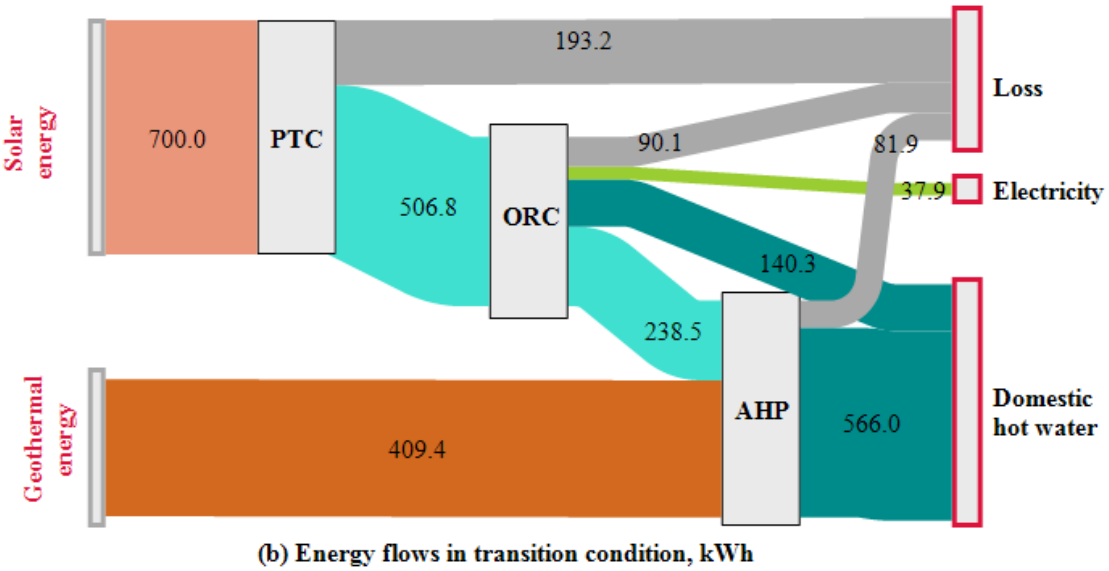

(b) Energy flows in transition condition, kWh

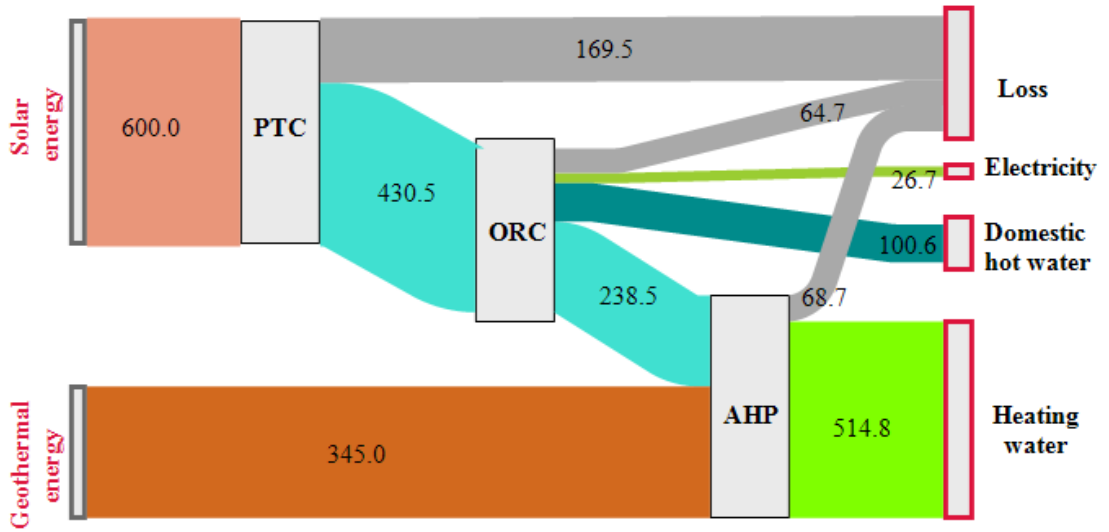

(c) Energy flows in heating condition, kWh

Fig. 3 Energy flow diagram of the different working conditions: (a) cooling, (b) transition, (c) heating.

The energy efficiency of each unit and output shares of the products are illustrated in Fig. 4. The energy efficiency of the AHP is the highestwith a value >85%, while the energy efficiency of the ORC is < 40%. However, compared to the assessment method in [32], the efficiency of the ORC is here higher, because the released heat in the condenser of the ORC is lost, while here it is utilized to produce domestic hot water. Comparing the energy efficiency of ORC in different conditions, the ORC in the cooling mode has the highest efficiency (39.3%), while the lowest value is 2 in the heating mode (9.6%). This can be explained by the higher solar output at higher outlet temperature from the PTC, which has a positive impact on the energy performance of the ORC.

Analyzing the output shares of the products in Fig. 4(b), the electricity share reaches the lowest

values for three modes: 8.8%, 5.1%, and 4.2%. The domestic hot water corresponds to 94.9% of the output in transition conditions, because of the contributions from both the AHP and the ORC. The chilled water and heating water are responsible for 33.5% and 41.5% of the total outputs in the cooling and heating modes.

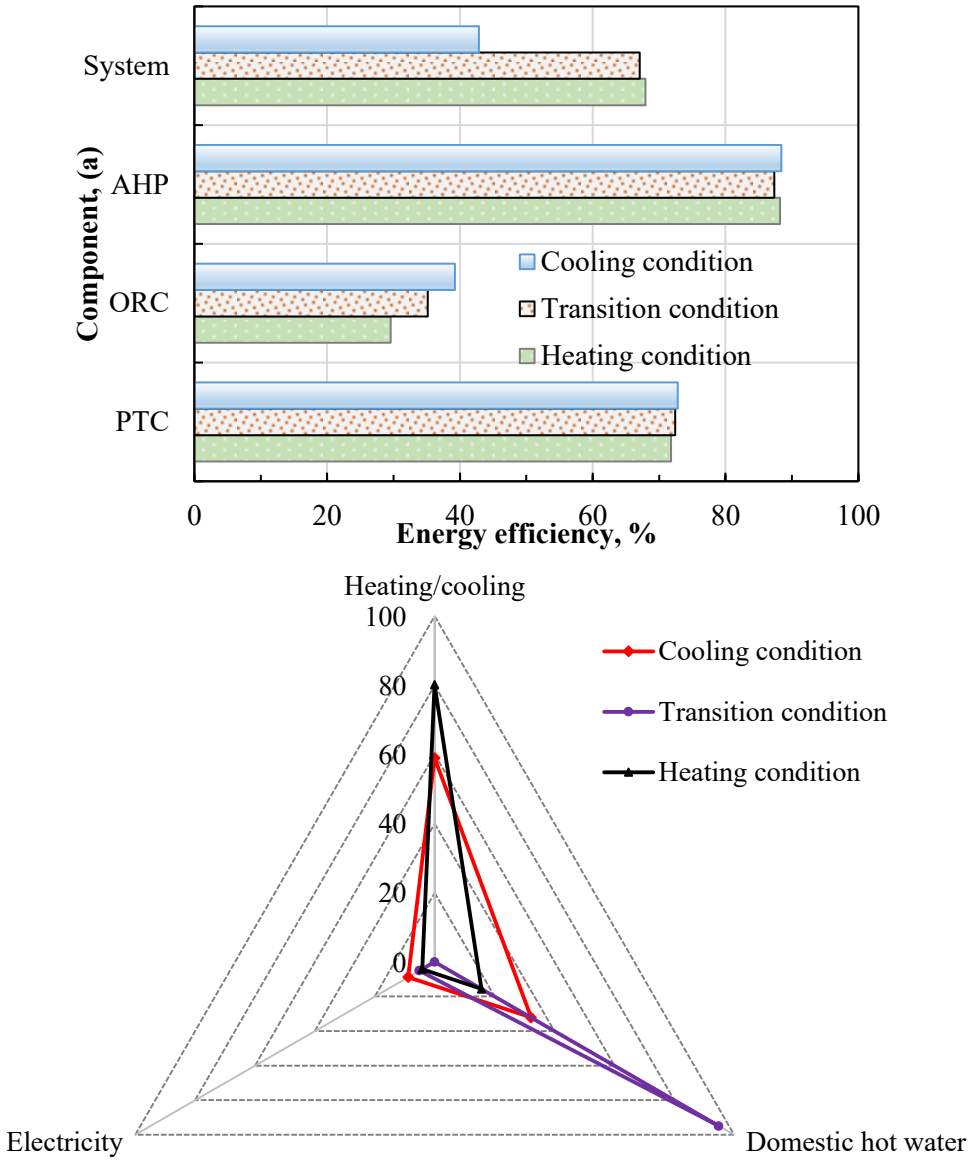

(b) Energy ratios of products in different conditions, %

Fig. 4 Energy efficiencies of subsystems and energy shares of the products.

4.2.4 Exergy performance in different conditions

The exergy flow diagrams of the three modes are shown in Fig. 5. Contrary to the energy flows in Fig. 3, most of the exergy loss flows to the environment. In the PTC unit, 73.6%, 74.4%, and 75.3% of the exergy is lost to the environment, and the useful exergy of solar steam is < 200 kWh. Moreover,

the loss of the PTC corresponds to the highest share of the total exergy loss of the system with a share of 76.7%, 80.8%, and 86.6%. The AHP and ORC are only responsible for < 25%. In the ORC-unit, the exergy of electricity is almost 11 times the exergy of the domestic hot water due to the lower temperature of water. The input solar exergy to the AHP is only 29.5% of the solar thermal energy, or 238.5 kWh in Fig. 3. Moreover, the geothermal exergy is much lower than the geothermal energy consumption. Compared to the total exergy output, the cooling mode has a maximum value of 80.6 kWh exergy output, while the system in the heating mode reaches a minimum of 49.9 kWh. Analyzing the water products, the chilled water has the. highest exergy capacity of 27.0 kWh, while the exergy of the domestic hot water in the transition mode is the lowest, or, 17.2 kWh, although it is the only water product in transition conditions.

The exergy efficiency of the PTC solar thermal units is higher than the exergy efficiency of photovoltaic/thermal collectors [49] and evacuated tube collectors [44], while the ORC yields a lower electrical efficiency.

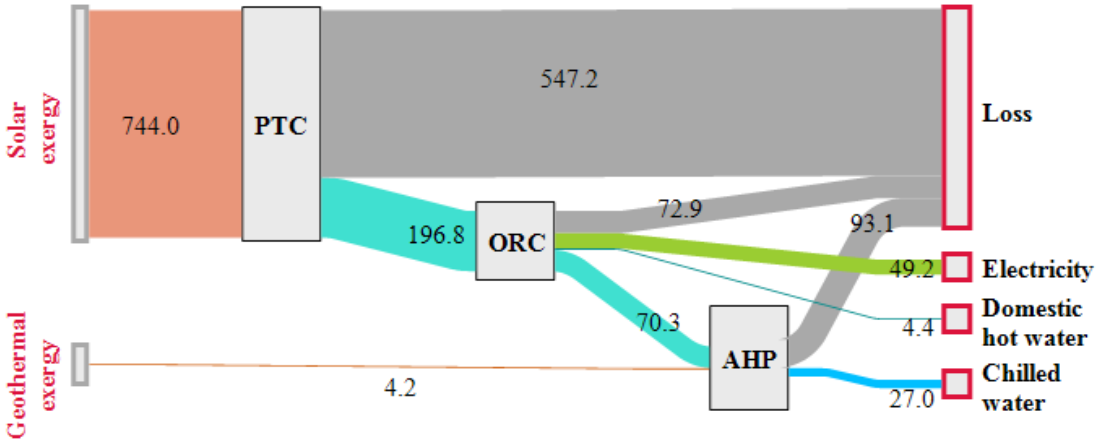

(a) Exergy flows in cooling condition, kWh

.0

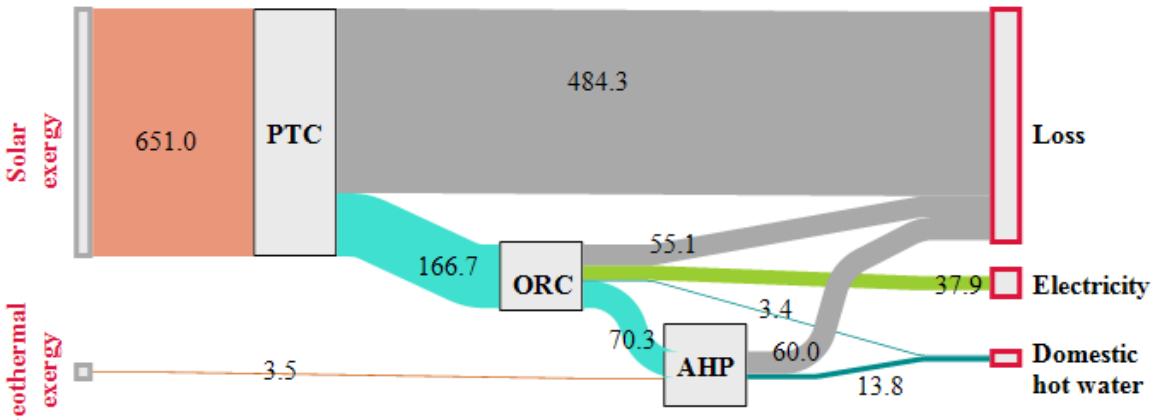

(b) Exergy flows in transition condition, kWh

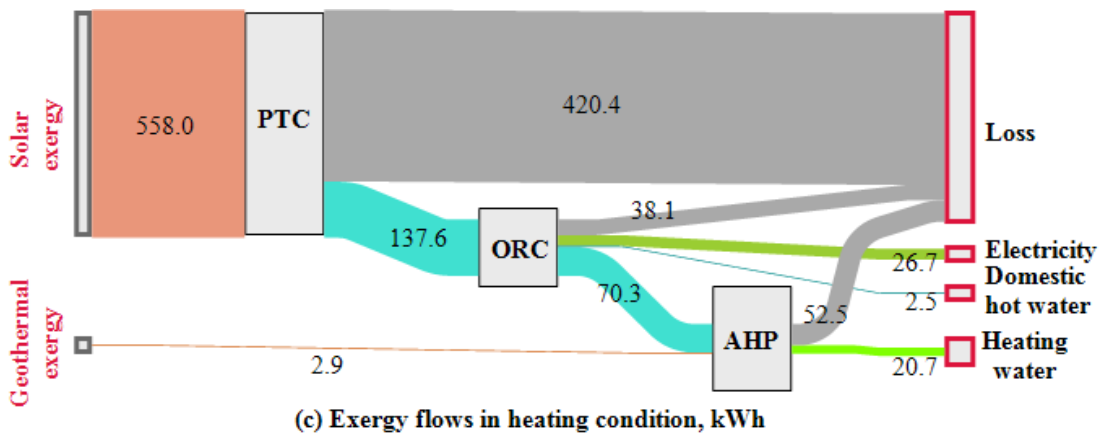

Fig. 5 Exergy flow diagram in different working conditions: (a) cooling, (b) transition, (c) heating.

The exergy efficiency and the exergy allocation share are displayed in Fig. 6. In Fig. 6(a), the exergy efficiencies of the PTC are close to 25% in all three operational modes. For the other components, the maximum exergy efficiency of the AHP is 28.3% in the heating mode, while the lowest in the cooling mode, or 4.3%. This can be explained by the working principles of the AHP in the cooling mode (Table 1), the geothermal exergy, 4.2 kWh, is a sum of the absorbed heat in chilled water and solar steam, while the domestic hot and space heating water are the products of the AHP in transition and heating modes. For the ORC-unit, the exergy efficiencies in the three modes are 27.2%, 24.8%, and 21.2%, respectively. It can be found that higher the solar steam temperature (state 2) in Fig. 1 results in a higher exergy efficiency, and is positive to the exergy outputs of the ORC including the domestic hot water and electricity. The exergy efficiency of the hybrid CCHP system is 9%.

Contrary to Fig. 4(b), the exergy share of the electricity is the highest , or, 61.0%, 68.8%, and 53.5% in the three modes. The domestic hot water share is the lowest due to lower exergy production. The share of the chilled water and heating water is 33.5% and 41.5% in the cooling and heating modes, respectively.

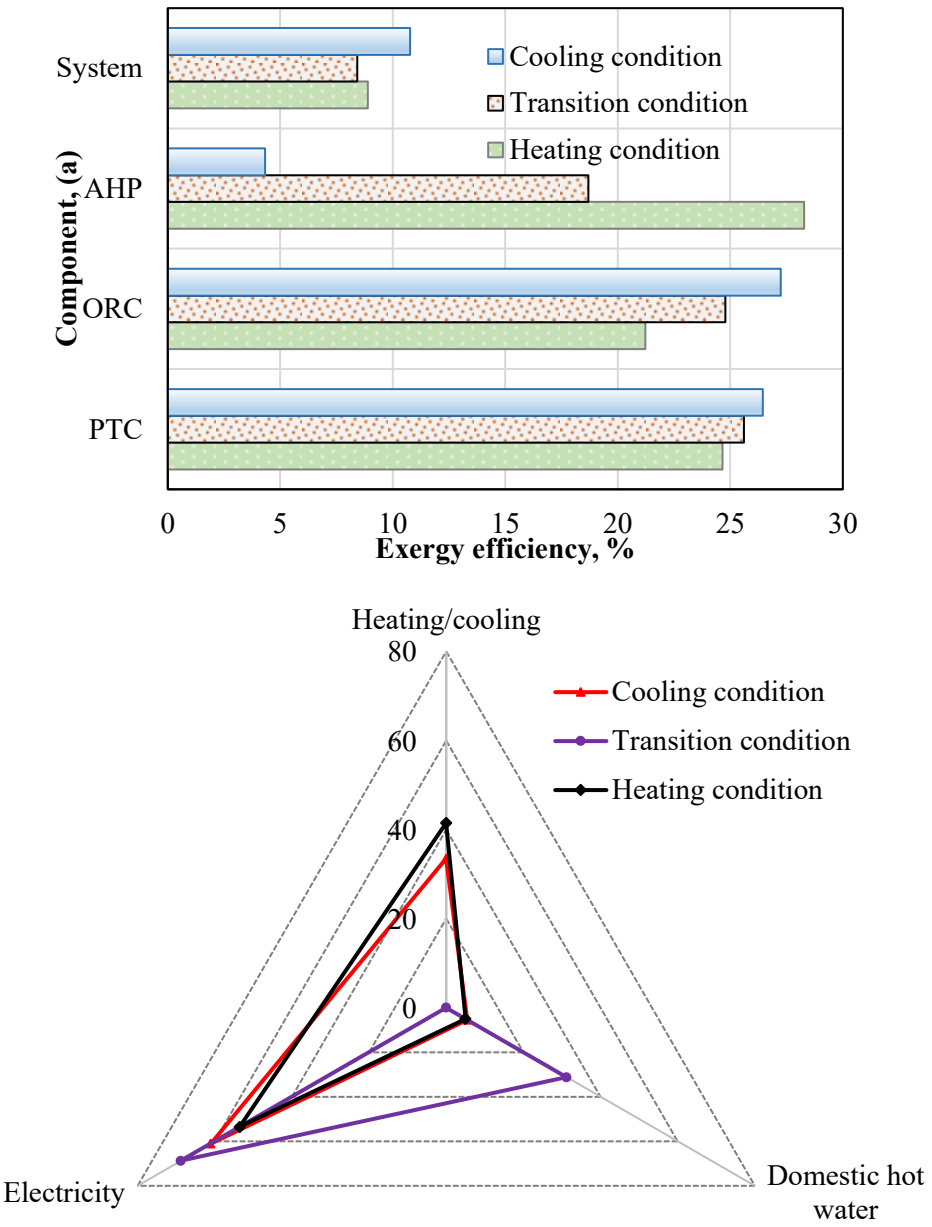

(b) Exergy ratios of products in different conditions, %

Fig. 6 Exergy efficiencies of subsystems and product shares.

4.2.5 Exergo-economic cost performance analysis in different conditions

The exergo-economic cost diagram for the three operational modes is shown in Fig. 7. The exergy cost performance of a certain component is related to its levelized and fuel cost (Eq. 10). For the PTC-unit, the solar radiation is free of cost. The initial investment costs of the three units of the proposed CCHP system are determined in standard conditions (1000 W/m^2, 25°C), yielding as the levelized costs of PTC, ORC, and AHP 2.59 \$/h, 4.80 \$/h, and 1.97 \$/h, respectively. For the whole system, the total

component cost is 5.6, 6.8, and 8.1 times the fuel cost (geothermal cost), and the geothermal cost is the lowest one, or 1.16 $/h in heating mode. Compared to other products, the cost of domestic hot water from the ORC is very low, < 0.1 $/h, while the other costs are> 3 $/h, including the domestic heat from the AHP in transition conditions. The reason is the lowest energy level of domestic hot water (Eq. 17), which is caused by the lower temperature. On the other hand, the product cost from AHP is higher than the cost of electricity from ORC, although the energy level of electricity is the highest, 1. This is because the AHP works behind the ORC unit, and only one product is carried out. Thus, the product cost from AHP is equal to the sum of geothermal cost, component cost and steam cost from ORC. Contrary to the exergy cost flow of fossil fuel fired units [44, 49], the PTC only includes the exergy cost of the installation process, while the exergy cost consumption of natural gas is nearly 3 times the cost of the installation stage.

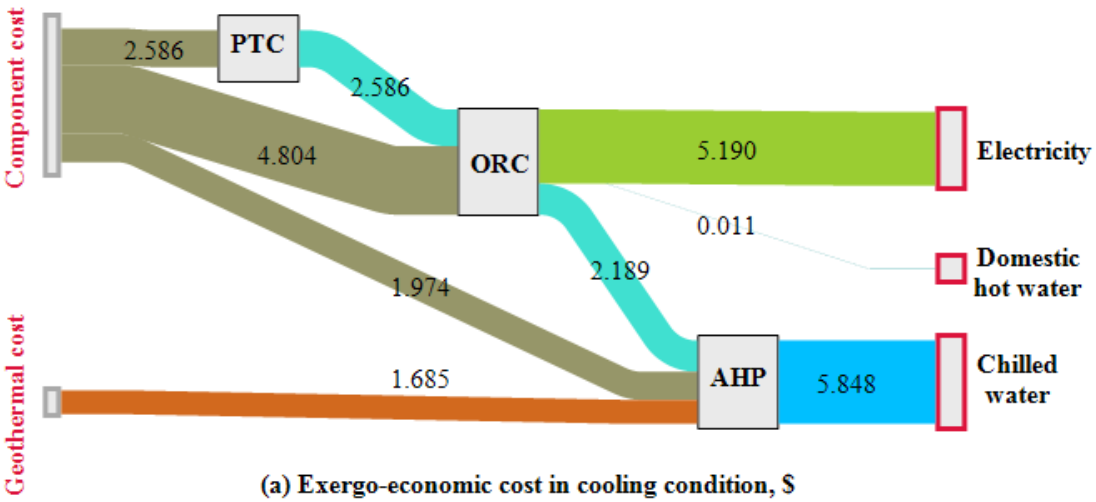

(a) Exergo-economic cost in cooling condition, $

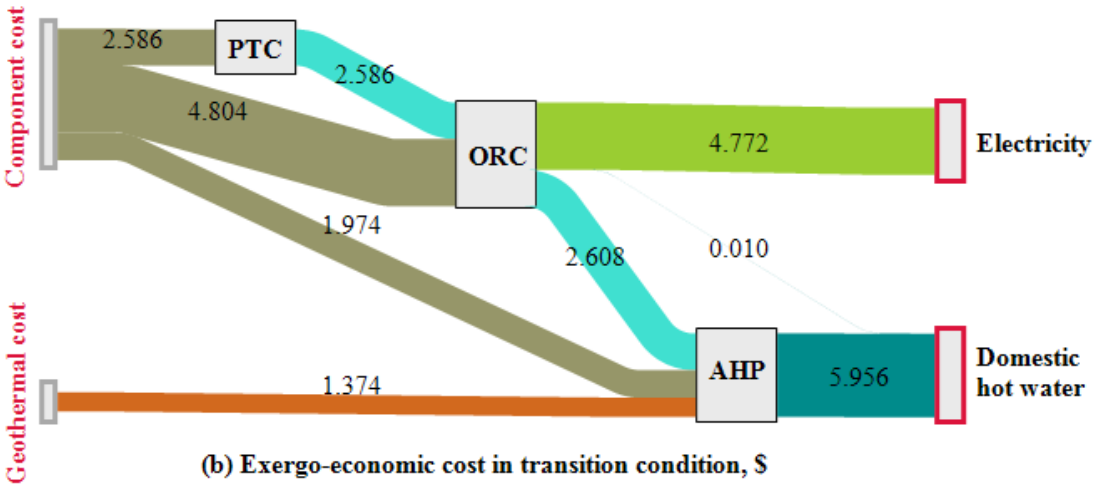

(b) Exergo-economic cost in transition condition, $

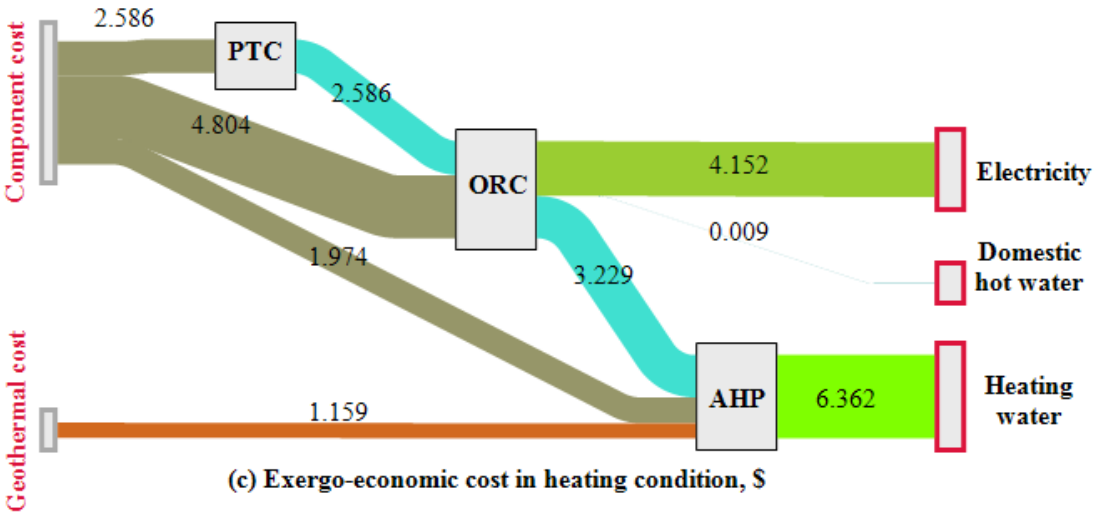

Fig. 7. Exergo-economic cost flow (per hour) diagram in different working conditions: (a) cooling, (b) transition, (c) heating mode.

5 Sensitivity analysis

The energy, exergy and exergo-economic analyses carried out in Section 4.2 were based on assumptions such as operational shares, yearly solar irradiance, and other parameters. It is therefore useful to evaluate the performance sensitivity against these parameters.

5.1 Impact of cooling and heating operating share

The share of operating modes are related to the operating hours in different conditions (Eq. 1). With a constant yearly solar irradiance in Fig. 2, the different operating shares correspond to different operating hours. We have assumed that the cooling and heating share varies between [0, 0.5], and the corresponding results of energy, exergy and specific exergo-economic are shown in Fig. 8.

A higher cooling share (ε_{cool}) results in a lower energy efficiency, whereas it increases the exergy efficiency (Figs. 8a-b). With a higher ε_{cool}, the contribution of the cooling mode is higher, and the energy efficiency is lower, while the exergy efficiency in cooling is larger than in the other modes. As ε_{cool} raises 0.1 units, the energy and exergy efficiencies change by 0.40% and 0.27% when ε_{heat} = 0. The ε_{heat} has a lower impact on energy and exergy performance: Within the full range of ε_{heat}, the efficiencies vary by 0.46% and 0.21% (ε_{cool} = 0).

Analyzing the specific costs of chilled and heating water in Figs. 8 c-d, increasing ε_{cool} raises the specific cost of chilled and heating water, while ε_{heat} has an opposite effect. With a higher ε_{cool} or ε_{heat}, the operating hours of the hybrid CCHP system decrease or increase, because the solar irradiance in the cooling and heating modes is 800 W/m^2 and 600 W/m^2, respectively. With a constant ε_{cool}= 0.5, the cost of chilled and heating water decrease 4.9%, and 5.6% over the whole range of ε_{heat}. When ε_{heat} = 0.5, the cost of the two water products increase 5.4%, and 6.3%.

ε_{cool} decreases the specific cost of electricity, while ε_{heat} raises it linearly. Compared to the other two conditions, the specific cost in the cooling mode is the lowest, although the levelized component cost increases through the reduced yearly operating hours with a higher ε_{cool}. Over the range of ε_{cool} and ε_{heat}values considered, the maximum and minimum cost of electricity is 0.13 \$/kWh and 0.12 \$/kWh.

From Fig. 8(f), increasing ε_{cool} and ε_{heat} have a similar impact on the cost of domestic hot water: As the shares raise, the specific cost decreases slowly and then increases faster with a higher share. During the cooling and heating modes, the domestic hot water from the ORC-unit has the lowest specific cost due to its lowest energy level and lower component cost. However, in the transition condition, the AHP-unit generates domestic hot water at a higher cost as it is the only product of the AHP. Thus, a higher $\varepsilon_{transition}$ means a higher cost of domestic hot water. The maximum cost is 0.34 \$/kWh when $\varepsilon_{transition}$ = 1.

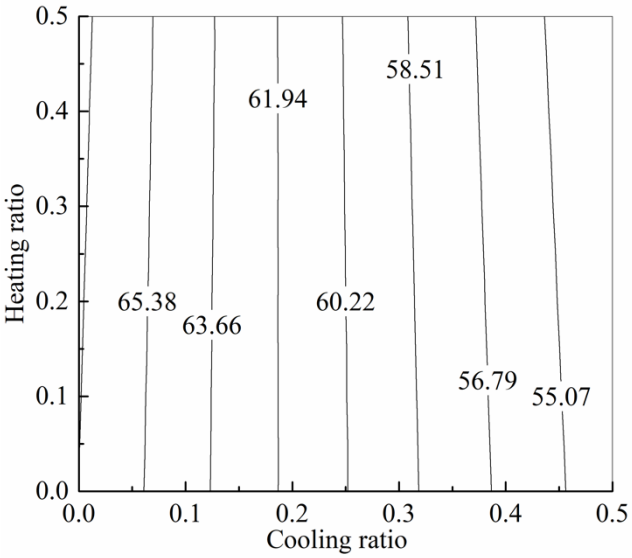

(a) Energy efficiency, %

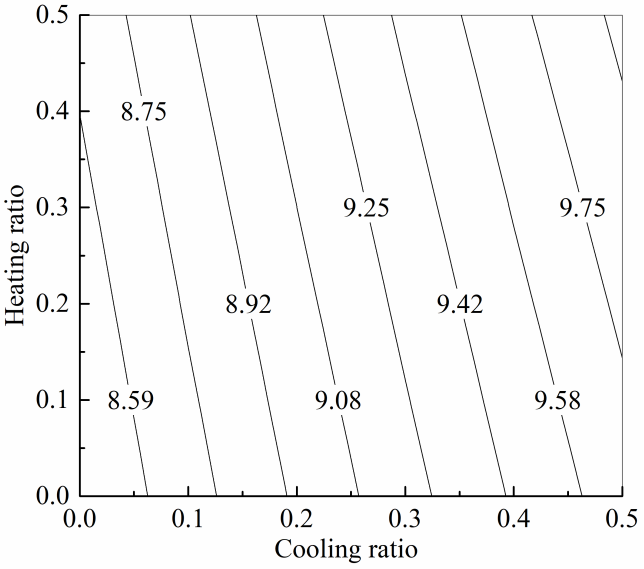

(b) Exergy efficiency, %

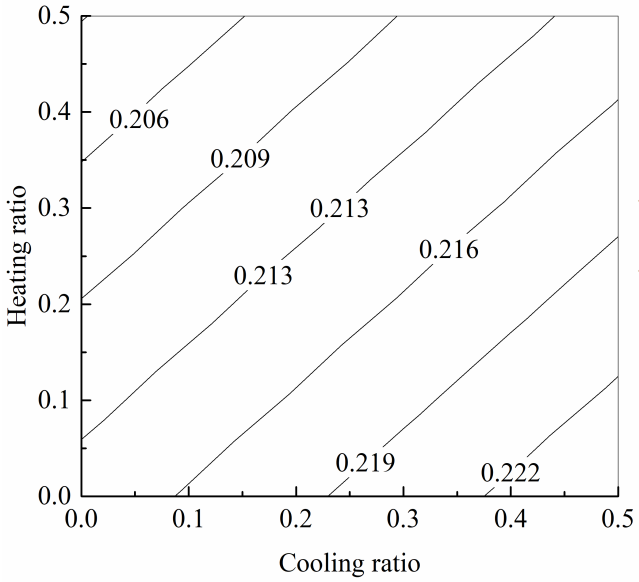

(c) Specific cost of chilled water, $/kWh

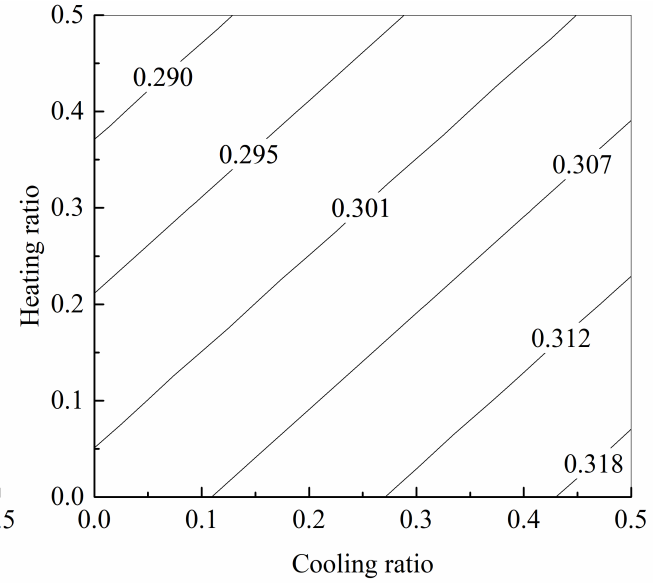

(d) Specific cost of heating water, $/kWh

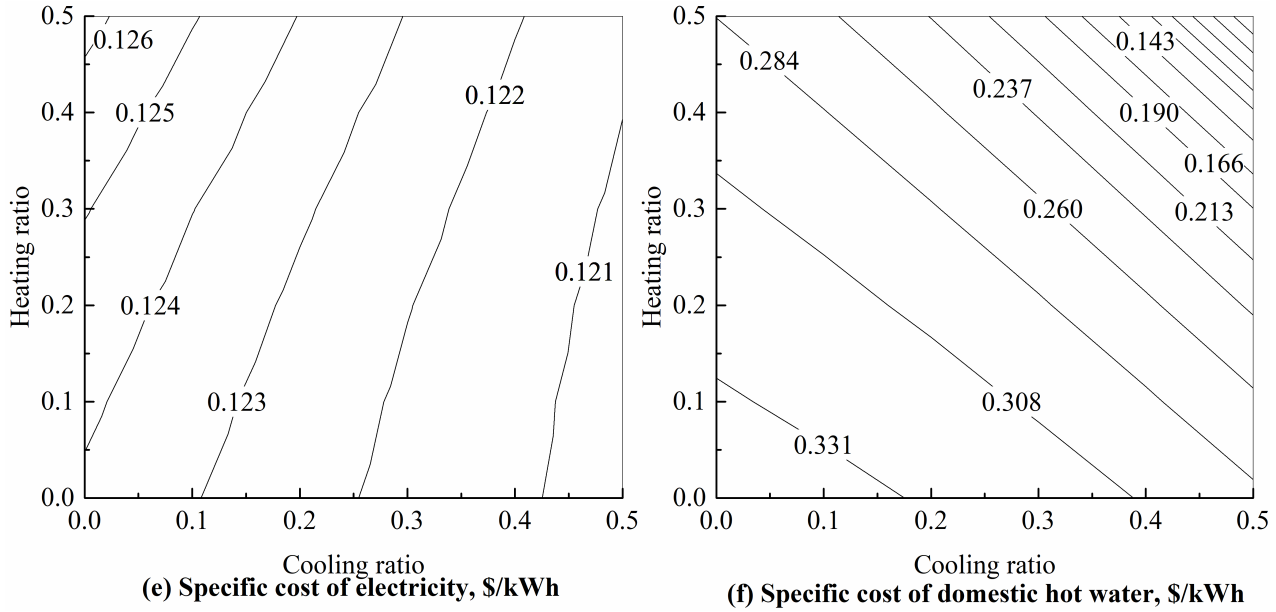

Fig. 8 Variation of efficiencies and specific costs of products as a function of the cooling and heating shares.

5.2 Impact of outlet solar steam temperature from the ORC

In Section 2, the inlet (T3) and outlet (T1) temperatures of the AHP unit were set at 170°C and 130°C. The sensitivity analysis of these two temperatures is shown in Fig. 9.

With a higher inlet temperature (T1) of the PTC, the energy efficiency decreases due to lower thermal output from PTC, while the exergy efficiency of the PTC increases from the higher outputs of products. When T3 = 170°C, the energy efficiency decreases 2.2% when the T1 increases 10°C and the exergy efficiency rises by 0.64%. On the other hand, when T3=130°C, the efficiency varies 3.6%, and 4.9%.

Form Fig. 9(c), with higher T1 and constant T3 (170°C), the specific cost of chilled water varies from 0.20 $/kWh to 0.23 $/kWh, and improves with an increasing gradient. With constant T3, the solar input to the AHP decreases when T1 increases. The component cost of the AHP will decline at the same time, but the cost of the inlet steam increases due to the higher component cost of the ORC. The trend is also similar with he cost of the heating water in Fig. 9(d). Compared to the impacts of T1, the contributions of T3 on the specific cost of chilled and heating water are lower.

The variation of electricity as a function of T1 and T3 is shown in Fig. 9(e) Both higher T1 and T3 decrease the cost of electricity at different levels. When T3 = 170°C or T1 = 130°C, the cost of

electricity decreases 2.4% or 6.2%. It can be concluded that the exergo-cost of electricity is more sensitive to the variation of T3, but less to T1. The cost of domestic hot water (Fig. 9f) decreases with higher T1. However, the T3 has an opposite impact on the cost of domestic hot water: as T1 = 130°C, the cost increases by 0.10 $/kWh.

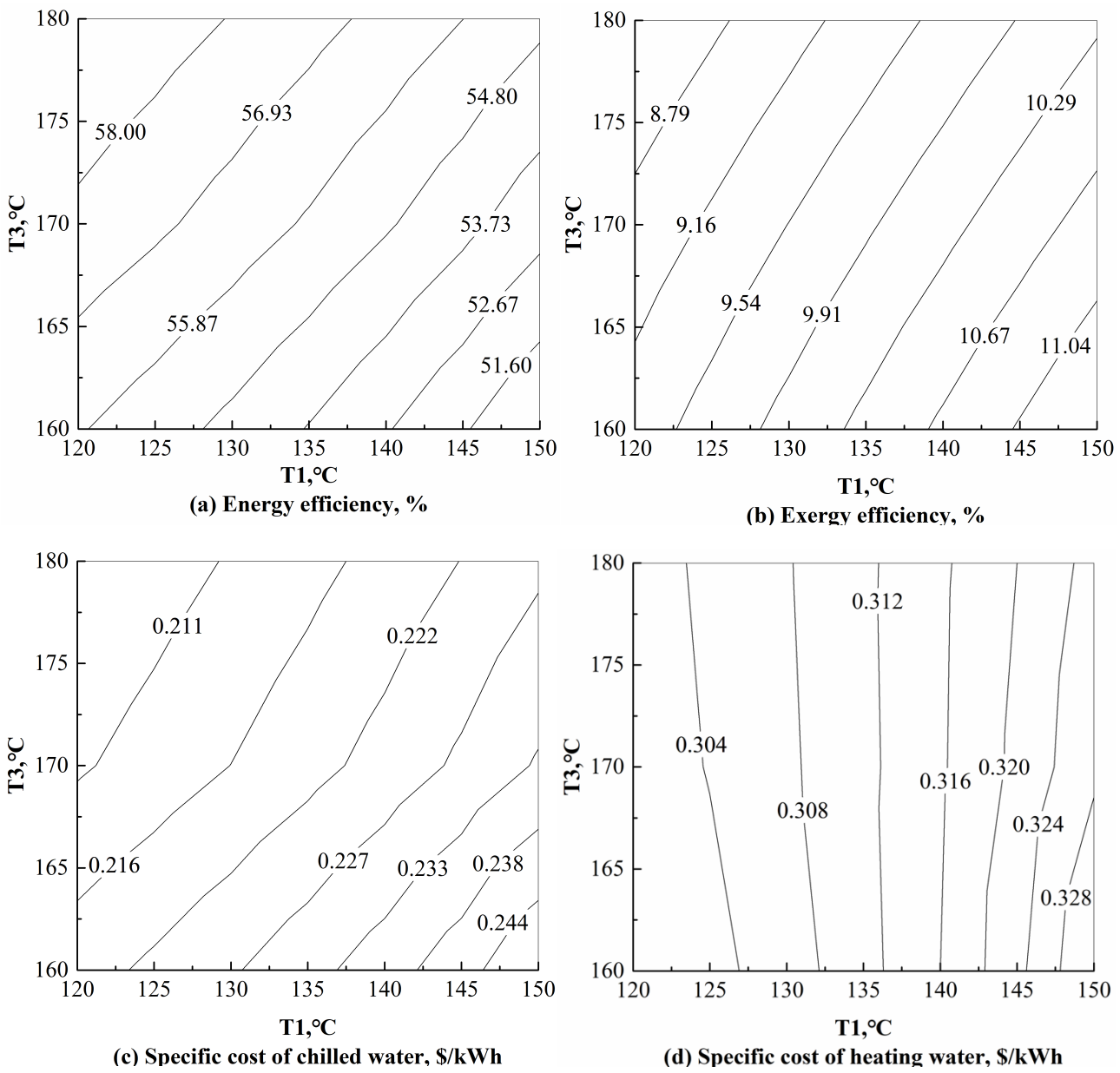

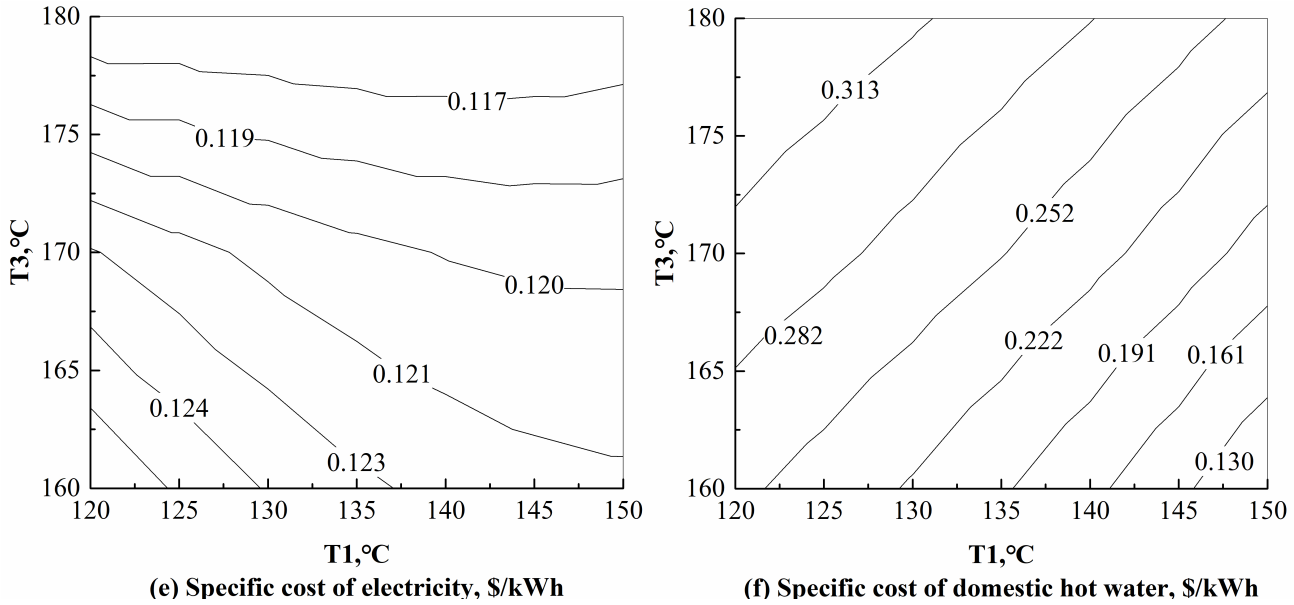

Fig. 9 Variation of efficiencies and specific costs of products as function of solar steam temperature (T1 and T3).

5.3 Impact of solar irradiance

The yearly solar irradiance varies from year to year. Here we evaluate the impact on specific costs when the solar irradiance varies from -30% to +30% shown in Fig. 10.

At higher irradiance conditions, the operating hours increase which results in a decreasing levelized hourly investment cost. Furthermore, the costs of the four products decrease steeply. For the whole range shown in Fig.10, the cost of chilled water, electricity, heating water, and domestic hot water decreases 36.0%, 46.2%, 40.5%, and 38.2%, respectively.

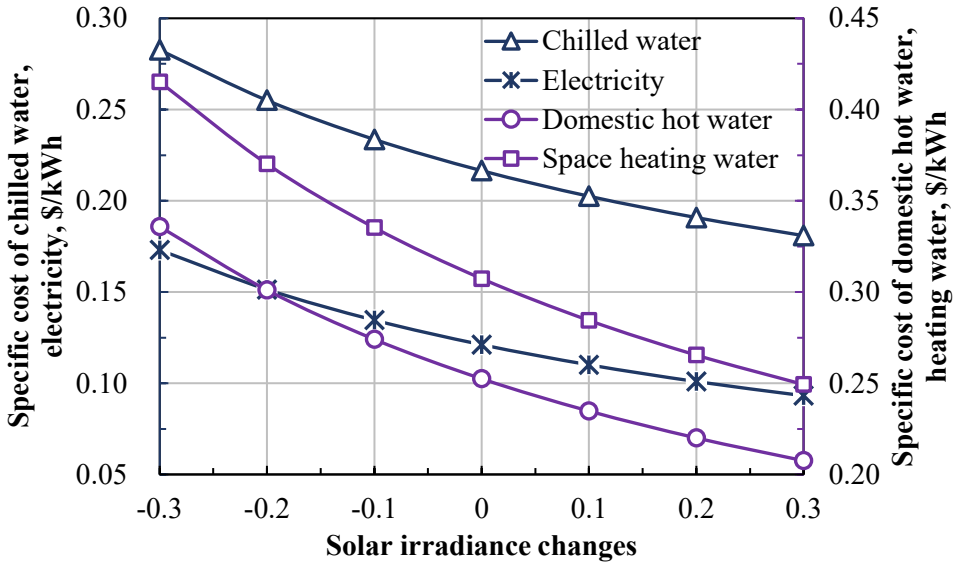

Fig. 10. Variation of specific costs of products as function of solar irradiance change.

5.4 Impact of condensation temperature of ORC

The condensation temperature is an essential parameter in the ORC-unit, which can influence the energy and exergy outputs, the heat transfer area of condenser needed, and the exergo-economic performance. The impact of the condensation temperature on the performance of hybrid CCHP system are shown in Fig. 11.

In Fig. 11(a), the energy efficiency drops linearly, but very little with increasing condensation temperature. The output of domestic hot water from the ORC increases, while the electricity output decreased more a little. On the other hand, the exergy efficiency decreases from 10.1% to 9.0%, as the temperature rises from 50°C to 70°C. This can be attributed to the slower increase of domestic hot water exergy, but higher reduction of electricity exergy.

The variation of the specific cost of multi-products is shown in Fig. 11(b). The condensation temperature has a lower influence on the exergo-economic costs. For the whole temperature range, the costsof chilled water, domestic hot water, heating water, and electricity raise by 0.004 $/kWh, 0.001 $/kWh, 0.003 $/kWh, and 0.005 $/kWh, respectively.

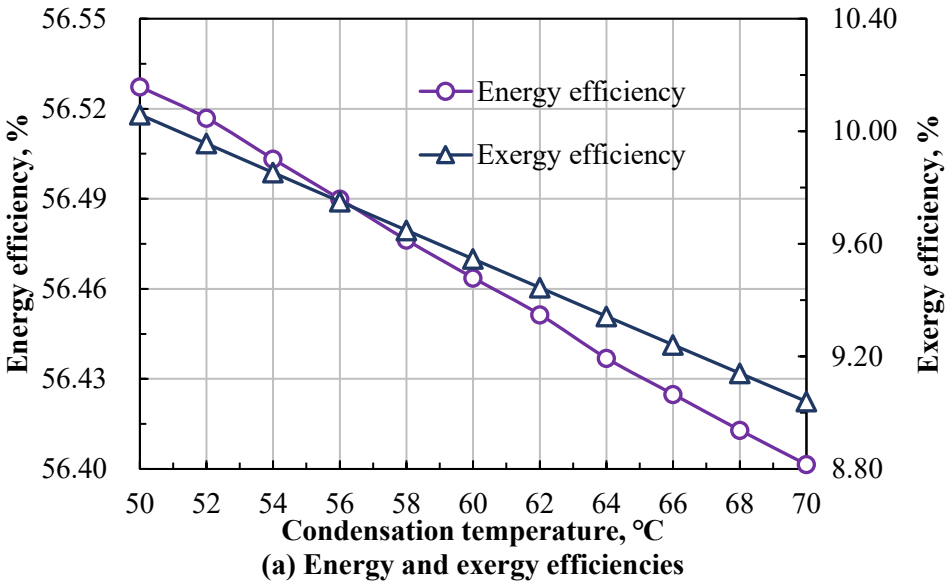

(a) Energy and exergy efficiencies

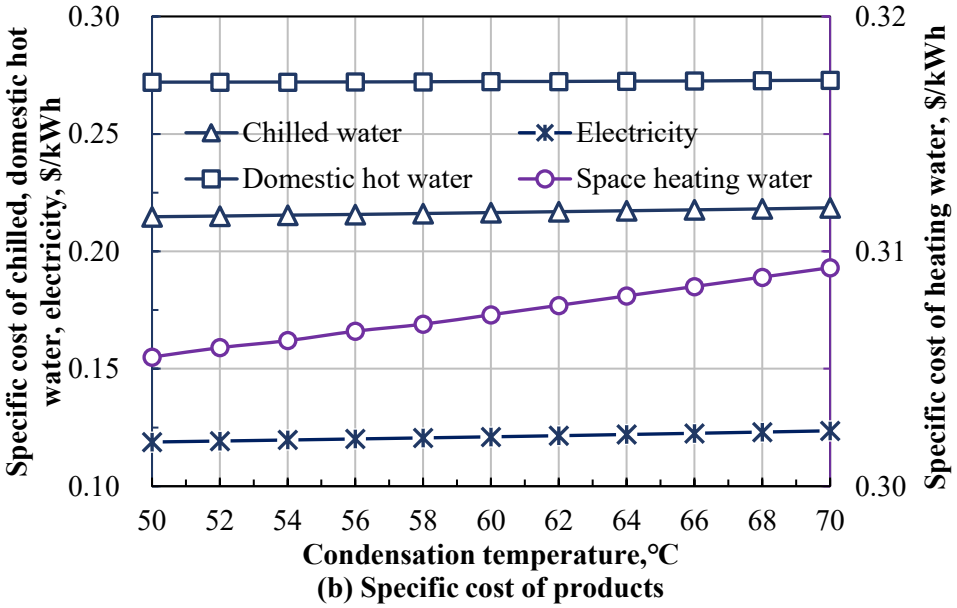

Fig. 11 Variation of efficiencies and specific costs of products as function of condensation temperature of ORC.

6 Conclusions

A novel combined cooling, heating and power (CCHP) system driven by parabolic trough collectors (PTC) is presented. In addition, geothermal energy is utilized as lower-grade heat. The system employs an organic Rankine cycle (ORC) unit to generate domestic hot water and electricity, and an absorption heat pump (AHP) to generate cooling, space heating, and domestic hot water for all conditions during the year. This system can well cascade the use of solar heat, and demonstrates a new direction of effective renewable energy utilization. Comprehensive energy, exergy, and economic performance analyses for different operational conditions werecarried out. The main conclusions are the following:

(1) The AHP-unit can well utilize solar and geothermal heat reaching a coefficient of performance of 1.38, 2.37, and 2.16 in cooling, transition and heating conditions. In cooling conditions, the energy efficiency is at lowest (42.8%), but reaches maximum exergy efficiency (10.8%), while the exergy efficiencies in other two modes are < 10%.

(2) The simple payback-time of the proposed CCHP system is 3.5 years. The specific exergy cost of space heating, domestic hot water, chilled water, and electricity are 0.31 $/kWh, 0.27 $/kWh, 0.22 $/kWh, and 0.12 $/kWh, respectively. The specific cost of the domestic hot water from the ORC is the

lowest of all (< 0.01 $/kWh) because of the lowest energy level of hot water and lower component cost.

Based on the sensitivity analysis done, the following key observations were done:

(1) The share of the cooling has a positive influence on the exergy efficiency, but a negative impact on the energy performance due to a lower energy efficiency in the cooling mode. Except for the exergy cost of electricity and domestic hot water, the increasing cooling share reduces the specific costs of the energy products, while the heating condition share can only raise the specific electricity cost.

(2) The inlet temperature of the PTC (T1) decreases the specific cost of electricity and domestic hot water, but improves the cost of chilled and heating water. Increasing the inlet temperature of the AHP (T3) has a negative impact on the economic performance of the domestic hot water, but has a lower impact on the heating water. Increasing T3 decreases the cost of chilled water and electricity steeply.

(3) Higher yearly solar irradiance leads to lower specific costs due to a decreasing component unit cost as the yearly operating hours increase. An increasing condensation temperature drops the efficiencies of performance, and slightly increases the cost of the products.

Future research could include multi-objective optimization of the system and analysis of the operating strategies of the district energy system coupled with energy storage and different renewable sources as well as sustainability analysis of these energy systems.

Acknowledgements

This research has been supported by National Natural Science Foundation of China (Grant No. 51736006).

Reference

[1] Klemm C, Vennemann P. Modeling and optimization of multi-energy systems in mixed-use districts: A review of existing methods and approaches. Renewable and Sustainable Energy Reviews. 2021;135:110206.

[2] Huang J, Fan J, Furbo S. Feasibility study on solar district heating in China. Renewable and

Sustainable Energy Reviews. 2019;108:53-64.

[3] Wang C, Li W, Li Z, Fang B. Solar thermal harvesting based on self-doped nanocermet: Structural merits, design strategies and applications. Renewable and Sustainable Energy Reviews. 2020;134:110277.

[4] Freitas S, Brito MC. Non-cumulative only solar photovoltaics for electricity load-matching. Renewable and Sustainable Energy Reviews. 2019;109:271-83.

[5] Singh M, Sinha I. Halide perovskite-based photocatalysis systems for solar-driven fuel generation. Solar Energy. 2020;208:296-311.

[6] Verma SK, Gupta NK, Rakshit D. A comprehensive analysis on advances in application of solar collectors considering design, process and working fluid parameters for solar to thermal conversion. Solar Energy. 2020;208:1114-50.

[7] Lakshika KAH, Boralessa MAKS, Perera MK, Wadduwage DP, Saravanan V, Hemapala KTMU. Reconfigurable solar photovoltaic systems: A review. Heliyon. 2020;6(11):e05530.

[8] Ruiz J, Martínez P, Sadafi H, Aguilar FJ, Vicente PG, Lucas M. Experimental characterization of a photovoltaic solar-driven cooling system based on an evaporative chimney. Renewable Energy. 2020;161:43-54.

[9] Chen Y, Wang J, Lund PD. Sustainability evaluation and sensitivity analysis of district heating systems coupled to geothermal and solar resources. Energy Conversion and Management. 2020;220:113084.

[10] Yuanjing W, Cheng Z, Yanping Z, Xiaohong H. Performance analysis of an improved 30 MW parabolic trough solar thermal power plant. Energy. 2020;213:118862.

[11] Ma Z, Li M-J, He Y-L, Zhang KM. Effects of partly-filled encapsulated phase change material on the performance enhancement of solar thermochemical reactor. Journal of Cleaner Production. 2021;279:123169.

[12] Sadeghi M, Yari M, Mahmoudi SMS, Jafari M. Thermodynamic analysis and optimization of a novel combined power and ejector refrigeration cycle – Desalination system. Applied Energy. 2017;208:239-51.

[13] Kasaeian A, Nouri G, Ranjbaran P, Wen D. Solar collectors and photovoltaics as combined heat and power systems: A critical review. Energy Conversion and Management. 2018;156:688-705.

[14] Kasaeian A, Bellos E, Shamaeizadeh A, Tzivanidis C. Solar-driven polygeneration systems:

Recent progress and outlook. Applied Energy. 2020;264:114764.

[15] Ullah KR, Saidur R, Ping HW, Akikur RK, Shuvo NH. A review of solar thermal refrigeration and cooling methods. Renewable and Sustainable Energy Reviews. 2013;24:499-513.

[16] Wang X, Xu Y, Bao Z, Li W, Liu F, Jiang Y. Operation optimization of a solar hybrid CCHP system for adaptation to climate change. Energy Conversion and Management. 2020;220:113010.

[17] Wang M, Wang J, Zhao Y, Zhao P, Dai Y. Thermodynamic analysis and optimization of a solar-driven regenerative organic Rankine cycle (ORC) based on flat-plate solar collectors. Applied Thermal Engineering. 2013;50(1):816-25.

[18] Zhang K, Chen X, Markides CN, Yang Y, Shen S. Evaluation of ejector performance for an organic Rankine cycle combined power and cooling system. Applied Energy. 2016;184:404-12.

[19] Parikhani T, Sattari Sadat SM. Multi-objective thermoeconomic optimization of innovative CCHP system driven by solar energy integrated with thermal energy storage. Energy. 2020:119410.

[20] Al-Mousawi FN, Al-Dadah R, Mahmoud S. Different bed configurations and time ratios: Performance analysis of low-grade heat driven adsorption system for cooling and electricity. Energy Conversion and Management. 2017;148:1028-40.

[21] Al-Mousawi FN, Al-Dadah R, Mahmoud S. Novel system for cooling and electricity: Four different integrated adsorption-ORC configurations with two expanders. Energy Conversion and Management. 2017;152:72-87.

[22] Al-Sulaiman FA, Dincer I, Hamdullahpur F. Exergy modeling of a new solar driven trigeneration system. Solar Energy. 2011;85(9):2228-43.

[23] Zhao L, Zhang Y, Deng S, Ni J, Xu W, Ma M, et al. Solar driven ORC-based CCHP: Comparative performance analysis between sequential and parallel system configurations. Applied Thermal Engineering. 2018;131:696-706.

[24] Jafary S, Khalilarya S, Shawabkeh A, Wae-hayee M, Hashemian M. A complete energetic and exergetic analysis of a solar powered trigeneration system with two novel organic Rankine cycle (ORC) configurations. Journal of Cleaner Production. 2020:124552.

[25] Haghghi MA, Pesteei SM, Chitsaz A, Hosseinpour J. Thermodynamic investigation of a new combined cooling, heating, and power (CCHP) system driven by parabolic trough solar collectors (PTSCs): A case study. Applied Thermal Engineering. 2019;163:114329.

[26] Chen Y, Zhao D, Xu J, Wang J, Lund PD. Performance analysis and exergo-economic

optimization of a solar-driven adjustable tri-generation system. Energy Conversion and Management. 2021;233:113873.

[27] Chen Y, Hua H, Wang J, Lund PD. Integrated performance analysis of a space heating system assisted by photovoltaic/thermal collectors and ground source heat pump for hotel and office building types. Renewable Energy. 2021.

[28] Ren F, Wei Z, Zhai X. Multi-objective optimization and evaluation of hybrid CCHP systems for different building types. Energy. 2021;215:119096.

[29] Wang X-Q, Li X-P, Li Y-R, Wu C-M. Payback period estimation and parameter optimization of subcritical organic Rankine cycle system for waste heat recovery. Energy. 2015;88:734-45.

[30] Soltani M, Chahartaghi M, Majid Hashemian S, Faghih Shojaei A. Technical and economic evaluations of combined cooling, heating and power (CCHP) system with gas engine in commercial cold storages. Energy Conversion and Management. 2020;214:112877.

[31] Gładysz P, Saari J, Czarnowska L. Thermo-ecological cost analysis of cogeneration and polygeneration energy systems - Case study for thermal conversion of biomass. Renewable Energy. 2020;145:1748-60.

[32] Tzivanidis C, Bellos E, Antonopoulos KA. Energetic and financial investigation of a stand-alone solar-thermal Organic Rankine Cycle power plant. Energy Conversion and Management. 2016;126:421-33.

[33] Li Z, Liu J. Appropriate heat load ratio of generator for different types of air cooled lithium bromide–water double effect absorption chiller. Energy Conversion and Management. 2015;99:264-73.

[34] Chen Y, Wang J, Ma C, Gao Y. Thermo-ecological cost assessment and optimization for a hybrid combined cooling, heating and power system coupled with compound parabolic concentrated-photovoltaic thermal solar collectors. Energy. 2019;176:479-92.

[35] Chen Y, Wang J, Lund PD. Thermodynamic performance analysis and multi-criteria optimization of a hybrid combined heat and power system coupled with geothermal energy. Energy Conversion and Management. 2020;210:112741.

[36] EuroTrough II: extension, test and qualification of EUROTROUGH from 4 to 6 segments at Plataforma Solar de Almeria. Project Cooordinator: Instalaciones Inabensa, S.A. April 2003.

[37] Herold K, Radermacher R, Klein S. Absorption Chillers and Heat Pumps, Second Edition ||

Double-Effect Water/Lithium Bromide Technology. 2016;10.1201/b19625:157-71.

[38] Chen Y, Hua H, Wang J, Lund PD. Thermodynamic performance analysis and modified thermo-ecological cost optimization of a hybrid district heating system considering energy levels. Energy. 2021;224:120067.

[39] Baidya D, de Brito MAR, Ghoreishi-Madiseh SA. Techno-economic feasibility investigation of incorporating an energy storage with an exhaust heat recovery system for underground mines in cold climatic regions. Applied Energy. 2020;273:115289.

[40] Jiang-Jiang W, Chun-Fa Z, You-Yin J. Multi-criteria analysis of combined cooling, heating and power systems in different climate zones in China. Applied Energy. 2010;87(4):1247-59.

[41] Wang J, Yang Y, Mao T, Sui J, Jin H. Life cycle assessment (LCA) optimization of solar-assisted hybrid CCHP system. Applied Energy. 2015;146:38-52.

[42] Lazzaretto A, Tsatsaronis G. SPECO: A systematic and general methodology for calculating efficiencies and costs in thermal systems. Energy. 2006;31(8):1257-89.

[43] Nazari N, Porkhial S. Multi-objective optimization and exergo-economic assessment of a solar-biomass multi-generation system based on externally-fired gas turbine, steam and organic Rankine cycle, absorption chiller and multi-effect desalination. Applied Thermal Engineering. 2020;179:115521.

[44] Wang J, Li S, Zhang G, Yang Y. Performance investigation of a solar-assisted hybrid combined cooling, heating and power system based on energy, exergy, exergo-economic and exergo-environmental analyses. Energy Conversion and Management. 2019;196:227-41.

[45] Boyaghchi FA, Chavoshi M, Sabeti V. Multi-generation system incorporated with PEM electrolyzer and dual ORC based on biomass gasification waste heat recovery: Exergetic, economic and environmental impact optimizations. Energy. 2018;145:38-51.

[46] Wang J, Li M, Ren F, Li X, Liu B. Modified exergoeconomic analysis method based on energy level with reliability consideration: Cost allocations in a biomass trigeneration system. Renewable Energy. 2018;123:104-16.

[47] Mussati SF, Gernaey KV, Morosuk T, Mussati MC. NLP modeling for the optimization of LiBr-H2O absorption refrigeration systems with exergy loss rate, heat transfer area, and cost as single objective functions. Energy Conversion and Management. 2016;127:526-44.

[48] EnergyPlus Energy Simulation Software.<https://www.energyplus.net/>.

[49] Wang J, Chen Y, Lior N. Exergo-economic analysis method and optimization of a novel photovoltaic/thermal solar-assisted hybrid combined cooling, heating and power system. Energy Conversion and Management. 2019;199:111945.

[50] Chen Y, Wang J, Ma C, Shi G. Multicriteria performance investigations of a hybrid ground source heat pump system integrated with concentrated photovoltaic thermal solar collectors. Energy Conversion and Management. 2019;197:111862.

[51] Haghghi MA, Mohammadi Z, Pesteei SM, Chitsaz A, Parham K. Exergoeconomic evaluation of a system driven by parabolic trough solar collectors for combined cooling, heating, and power generation; a case study. Energy. 2020;192:116594.

[52] Wang J, Mao T, Sui J, Jin H. Modeling and performance analysis of CCHP (combined cooling, heating and power) system based on co-firing of natural gas and biomass gasification gas. Energy. 2015;93:801-15.